Effects of Spike Shape on the Firing Dynamics and Synchronization Properties of Leaky Integrate and Fire Neurons with Dendritic Structure

Abulhair Saparov

April 23, 2013

Advisors: Michael A. Schwemmer, Professor Philip J. Holmes

Abstract

We study the effect of spike shape and dendritic properties on neuronal firing dynamics and synchronization. To do this, we present a multi-compartment leaky integrate-and-fire model of a neuron, which can effectively capture complex dendritic trees that passively transmit current. Due to the tractability of our model, we can derive the analytic solution in both spiking and non-spiking modes. We use the solution to construct the return map that captures the dynamics of the system, and we can characterize the excitability of the system in response to variations in the spike shape and dendritic properties. In the second part of the paper, we use the theory of weakly coupled oscillators to derive an equivalent phase model and phase response curve of our general system. This enables the examination of firing synchronization a system of two coupled multi-compartment LIF neurons. We use this to determine which spike shapes result in synchrony, anti-synchrony, or bistability, and the corresponding robustness of the phase-locking behavior.

Introduction

Neurons have highly intricate and extensive spatial structure, but are often modeled as single entities, with no explicit description of dendrites. Single-compartment models are incredibly useful, capturing a very wide range of neuronal phenomena [3]. However, biological neurons are much more spatially extensive, with potentially vast dendritic trees. This allows for greater heterogeneity in the structure and behavior of single neurons. For instance, the ion channel types and concentrations on the membrane can vary across dendrites and the axon of the same neuron [13, 14, 23], enabling richer firing patterns and behavior. Recent compartmental models of neurons show that the wide variety of firing patterns observed in neocortical neurons can be attributed to the dendritic structure [17]. It was shown that complex branching dendritic trees with certain properties can be represented equivalently using a single dendritic cable [19]. The dendritic cable model can be further simplified into a series of passively connected discrete compartments. Even a two-compartment leaky integrate-and-fire model captures complex behavior that a single compartment model cannot replicate [23]. Thus, in order to further examine the properties and more complex behaviors of dendritically-extended models, we focus on the multi-compartment description of neurons, in addition to

the effects of the passive compartments with various dendritic architectures. However, models with large numbers of compartments can also be difficult to work with, and so for our synchronization studies, we pay special attention to the two-compartment neuron.

Many models also typically model each spike as an all-or-nothing event, ignoring the complexity of a variable spike shape and its effects on the dynamics of the neurons. Although these models are successful in capturing a wide variety of behavior, there is evidence [6] that the stimulus can affect the spike shape and play an important role in the dynamics of neurons and neural networks. Mammalian central neurons express a very large number of diverse ion channels, which allows neurons to generate spikes with different shapes, frequencies, and patterns [2]. Additionally, Juusola et al. showed that spike codes that take advantage of variability in the spike shape have higher rates of information transfer and reliability. They found experimental evidence that suggests that biological neurons in the hippocampus utilize these non-classical spike codes [12]. This diversity in spiking behavior invariably contributes to the dynamics of the complex networks in the brain. Most models today ignore many of these effects, resulting in an oversimplification that may entirely remove computationally relevant dynamical behavior. For instance, the potential throughput of information transfer is limited if the variability in spike shape is overlooked. In our exploration, we will more closely examine how the dynamics and synchronization properties of neurons are affected by the variability of spike shapes.

Neurons can be coupled with either chemical or electrical connections. In the cortex, networks of inhibitory interneurons are electrically coupled with gap junctions. Although the importance of these gap junctions is not very well understood, electrical studies suggest that they play a role in helping to synchronize oscillatory behavior or generate particular neural rhythms [18, 10, 7]. In particular, the high incidence of gap junctions on the dendrites of cortical interneurons is thought to help coordinate synchronous oscillatory behavior [1]. Experimental studies have lent support for the existence of this dendro-dendritic electrical coupling, and theoretical studies have examined their dynamical consequences [15]. Most models of neural networks assume chemical coupling with synapses. However, the prevalence of gap junctions in the brain suggests that these models that ignore electrical coupling in neural circuits may also forgo important dynamical behavior, such as that related to firing synchronization. For example, it was shown that the robustness and stability of phase-locked states between two electrically-coupled ball-and-stick neurons is highly dependent on the location of the gap junction along the dendrite [21]. Here, we extend the work of Lewis and Rinzel to explore how the interaction between spike shape, dendritic properties, and electrical coupling affect the synchronization properties of the neuron.

This paper is divided into two overall parts. The goal of the first part is to understand how dendrites affect the firing dynamics of the multi-compartment leaky integrate-and-fire (LIF) neuron. To do so, we present a mathematical description of the multi-compartment leaky integrate-and-fire (LIF) neuron, focusing on two particular dendritic architectures: the first is in which the dendrites are aligned in a chain with the soma at one end, and the second is where each dendrite is attached directly to the soma. However, we will show that much of our analysis can be extended to arbitrary dendritic topologies. The solutions for both the non-spiking and spiking portions of the model are derived. These solutions are then used to construct a return map, which is a function that maps the state of each dendritic compartment at the end of the preceding spike to a state at the end of the next spike. This map reduces the dimensionality of the full system and enables closer examination of the spiking dynamics of the neuron. We use the map to search for changes in excitability. This enables the classification of firing behavior into Hodgkin's type I or type II excitability. A neuron classified as type I can fire at arbitrarily low oscillations near the onset of stable firing. For a type II neuron, the onset of periodic oscillations occurs with a nonzero frequency, and so there is a region of bistability where the initial state of the neuron determines whether it will fire periodically or

not [11]. A reasonable way to ascertain the excitability of a neuron is to examine the f-I curves of the cell, where the firing frequency of the neuron is varied against the injected somatic current, and they provide a concise illustration of the firing properties of the cell. We use these diagrams extensively in the results of the first part to determine the effects of varying the parameters of the model on the firing dynamics of the neuron. The width of the bistable region can be used to characterize excitability (the range of the value of injected current for which the neuron is bistable). This metric is easily discernible in these bifurcation diagrams, and so the effect of additional passive compartments can be ascertained. We also consider the differences between homogeneous and heterogeneous settings of parameters across dendrites. We find that dendritic properties can significantly change the firing dynamics of the system.

In the second part of this paper, we explore the synchronization dynamics of multi-compartment LIF neurons electrically-coupled at their dendrites. We assume that the neurons, when isolated, are in the stable periodic firing regime. We use the theory of weakly coupled oscillators [9, 24] to derive the phase model, which is a single scalar differential equation that describes the evolution of the phase difference of two multi-compartment LIF neurons electrically-coupled at their dendrites. This equation requires the specification of the infinitesimal phase response curve ($iPRC$), which describes how the phase of a spiking neuron responds to infinitesimal impulses of injected current. Owing to the tractability of our model, we are able to derive the general iPRC, in an analytical form, for every compartment in our model, allowing us to explore how the spike shape affects the response properties of each compartment in the model. As an example case, we examine the synchronization properties of two two-compartment neurons with electrical coupling at their dendrites. We explore the effect of changing spike shapes and dendritic properties on the phase-locking of the system. Finally, the robustness to heterogeneity in firing frequency of these phase-locked states in response to differences in the frequency between the coupled neurons is explored as in [21]. Spike shape has a significant effect on the existence, robustness, and stability of phase locking.

Model

The simple leaky integrate-and-fire neuron is extended by adding spherical dendritic compartments which exchange current with each other and the soma via passive diffusion. We present our multi-compartment leaky integrate-and-fire neuron initially by focusing on two dendritic topologies. The first we will call the "branch" model, where all n dendrites are attached to the soma and nothing else. The second model is called the "chain" model where all compartments are arranged in a linear chain, with each compartment being connected to at most two other compartments, and the soma is at one of the ends.

In the branch model, let $\bar{V}_i$ be the voltage of the i-th dendrite measured in mV, $\bar{V}_S$ is the somatic voltage measured in mV, C_m is the membrane capacitance measured in μF/cm^2, g_{LD_i} is the dendritic leakage conductance measured in mS/cm^2, E_{LD_i} is the leakage reversal potential of the i-th dendrite measured in mV, $\bar{I}_i$ is the injected dendritic current measured in μA/cm^2, g_{C_i} is the coupling conductance measured in mS, and A_i is the surface area of the dendritic compartment measured in cm^2. Then, the dendritic voltages are governed by the following differential equation:

$$C_m \frac{d\bar{V}_i}{d\bar{t}} = -g_{LD_i}(\bar{V}_i - E_{LD_i}) + \bar{I}_i + \frac{g_{C_i}}{A_i}(\bar{V}_S - \bar{V}_i) \tag{1}$$

When the neuron is not spiking, the somatic voltage is governed by the differential equation:

$$C_m \frac{d\bar{V}_S}{d\bar{t}} = -g_{LS}(\bar{V}_S - E_{LS}) + \bar{I}_S + \sum_i \frac{g_{C_i}}{A_S}(\bar{V}_i - \bar{V}_S) \tag{2}$$

Where g_{LS} is the somatic leakage conductance, E_{LS} is the somatic leakage reversal potential, $\bar{I}_S$ is the injected somatic current, and A_S is the surface area of the soma. We define $\bar{t}_s^j$ to be the j-th time at which the soma reaches the threshold potential $\bar{V}_{th}$ and the j-th spike is elicited. When the neuron spikes, however, the somatic potential is governed entirely by the spike shape $\bar{h}(\bar{t} - \bar{t}_s^j)$ where the spike begins at time $\bar{t}_s^j$:

$$\bar{V}_S(\bar{t}) = \bar{h}(\bar{t} - \bar{t}_s^j) \tag{3}$$

We fix the duration of the spike to $\bar{T}_a$, after which the neuron stops spiking, the somatic voltage is reset to the value $\bar{V}_R$, and the system continues to evolve.

In the chain model, we have a different set of differential equations. Note that the first $n-1$ dendrites are connected to both the preceding and subsequent dendrites, and the n-th dendrite is only connected to the previous compartment. Using the notation above, we write the equation for the voltage of dendrite $i \in [2, n-1]$:

$$C_m \frac{d\bar{V}_i}{d\bar{t}} = -g_{LD_i}(\bar{V}_i - E_{LD_i}) + \bar{I}_i + \frac{g_{C_i}}{A_i}(\bar{V}_{i-1} - \bar{V}_i) + \frac{g_{C_{i+1}}}{A_i}(\bar{V}_{i+1} - \bar{V}_i) \tag{4}$$

For the dendrites at the ends, we have:

$$\begin{aligned} C_m \frac{d\bar{V}_1}{d\bar{t}} &= -g_{LD_1}(\bar{V}_1 - E_{LD_1}) + \bar{I}_1 + \frac{g_{C_1}}{A_1}(\bar{V}_S - \bar{V}_1) + \frac{g_{C_2}}{A_1}(\bar{V}_2 - \bar{V}_1) \\ C_m \frac{d\bar{V}_n}{d\bar{t}} &= -g_{LD_n}(\bar{V}_n - E_{LD_n}) + \bar{I}_n + \frac{g_{C_n}}{A_n}(\bar{V}_{n-1} - \bar{V}_n) \end{aligned} \tag{5}$$

Finally, for the somatic membrane potential, we have:

$$C_m \frac{d\bar{V}_S}{d\bar{t}} = -g_{LS}(\bar{V}_S - E_{LS}) + \bar{I}_S + \frac{g_{C_1}}{A_S}(\bar{V}_1 - \bar{V}_S) \tag{6}$$

Similar to the branch model, the somatic potential is fully governed by the spike shape $\bar{h}(\bar{t} - \bar{t}_s^j)$ when the neuron is spiking.

Nondimensionalization

We nondimensionalize the system using the following substitutions, with $n = 1, 2, ..., S$:

$$V_n(t) = \frac{\bar{V}_n(\bar{t}/\tau_1) - E_{LD_1}}{\bar{V}_{th} - E_{LD_1}} \text{ and so } V_{th} = 1 \tag{7}$$

$$I_n = \frac{\bar{I}_n}{g_{LD_1}(\bar{V}_{th} - E_{LD_1})} \tag{8}$$

Parameters	
$\bar{V}_n$	membrane potential of compartment n
$\bar{I}_n$	current injected into compartment n
$\bar{t}$	dimensional time
C_m	membrane capacitance
g_{LD_i}	dendritic leakage conductance
g_{LS}	somatic leakage conductance
E_{LD_i}	dendritic leakage reversal potential
E_{LS}	somatic leakage reversal potential
A_n	surface area of compartment n
g_{C_i}	coupling conductance

Table 1: Lists each dimensional parameter and its physical significance.

$$\tau_i = \frac{C_m}{g_{LD_i}} \text{ where } \tau_S = \frac{C_m}{g_{LS}} \tag{9}$$

$$g_i = \frac{g_{C_i}}{A_S g_{LD_1}} \tag{10}$$

$$\alpha_i = \frac{A_S}{A_i} \tag{11}$$

$$\beta_i = \frac{E_{LD_i} - E_{LD_1}}{\bar{V}_{th} - E_{LD_1}} \text{ where } \beta_S = \frac{E_{LS} - E_{LD_1}}{\bar{V}_{th} - E_{LD_1}} \tag{12}$$

$$\gamma_{D_i} = \frac{g_{LD_i}}{g_{LD_1}} \text{ where } \gamma_S = \frac{g_{LS}}{g_{LD_1}} \tag{13}$$

Applying these transformations to the dimensional representation of the "chain" model yields the following non-dimensionalized system of differential equations:

$$\begin{aligned}
&\frac{dV_1^{chain}}{dt} = -V_1^{chain} + I_1 + \alpha_1 g_1 (V_S^{chain} - V_1^{chain}) + \alpha_1 g_2 (V_2^{chain} - V_1^{chain}) \\
&\frac{dV_i^{chain}}{dt} = -\gamma_i (V_i^{chain} - \beta_i) + I_i + \alpha_i g_i (V_{i-1}^{chain} - V_i^{chain}) + \alpha_i g_{i+1} (V_{i+1}^{chain} - V_i^{chain}) \\
&\qquad\qquad\qquad\qquad\qquad\qquad\qquad\qquad\qquad\qquad\qquad\qquad \text{for } i \in [2, n-1] \\
&\frac{dV_n^{chain}}{dt} = -\gamma_n (V_n^{chain} - \beta_n) + I_n + \alpha_n g_n (V_{n-1}^{chain} - V_n^{chain}) \\
&\begin{cases} \frac{dV_S^{chain}}{dt} = -\gamma_S (V_S^{chain} - \beta_S) + I_S + g_1 (V_1^{chain} - V_S^{chain}) & \text{if } t \notin (t_s, t_s^j + T_a] \\ V_S^{chain}(t) = h(t - t_s^j) & \text{if } t \in (t_s, t_s^j + T_a] \end{cases}
\end{aligned} \tag{14}$$

In the "branch" model, we nondimensionalize the system using the same transformations:

$$\begin{aligned}
&\frac{dV_i^{branch}}{dt} = -\gamma_i (V_i^{branch} - \beta_i) + I_i + \alpha_i g_i (V_S^{branch} - V_i^{branch}) \\
&\begin{cases} \frac{dV_S^{branch}}{dt} = -\gamma_S (V_S^{branch} - \beta_S) + I_S + \sum_{i=1}^{n} g_i (V_i^{branch} - V_S^{branch}) & \text{if } t \notin (t_s, t_s^j + T_a] \\ V_S^{branch}(t) = h(t - t_s^j) & \text{if } t \in (t_s, t_s^j + T_a] \end{cases}
\end{aligned} \tag{15}$$

Matrix formulation

The coefficients of the above dimensional and non-dimensional systems can be conveniently represented as matrices. This matrix formulation is sufficiently general to represent any dendritic topology, and we will conduct much of our analysis in this form. We re-write the non-dimensionalized system of differential equations in the following form:

$$\frac{d\mathbf{V}}{dt} = A^{NS}\mathbf{V} + \mathbf{b}^{NS} \qquad \text{if the neuron is not spiking} \tag{16}$$

Where A^{NS} is an $(n+1) \times (n+1)$ matrix of coefficients, $\mathbf{V}$ is a vector where the first n elements represent the non-dimensional dendritic voltage V_i, and the $(n+1)$-th element represents the non-dimensional somatic

voltage V_S.

$$\begin{cases} \dfrac{d\mathbf{V}_{dendrites}}{dt} = A^S \mathbf{V}_{dendrites} + \mathbf{b}^S(t) \\ V_S(t) = h(t - t_s^j) \end{cases} \qquad \text{if the neuron is spiking} \tag{17}$$

Where $\mathbf{V}_{dendrites}$ is an n-dimensional vector of non-dimensional dendritic membrane potentials. Here, A^S has one fewer row and column since the differential equation no longer governs the somatic voltage. We also define *biologically-realistic* settings of the parameters in our model to be such that all α, g, and γ are non-negative.

Non-spiking solution

If the neuron is not spiking, then the two models we presented are simply different ways to specify the matrix A_{NS} and vector $\mathbf{b}_{NS}$ in the system $\frac{d\mathbf{V}}{dt} = A_{NS}\mathbf{V} + \mathbf{b}_{NS}$ where for the "branch" model, we have:

$$A^{NS}_{branch} = \begin{bmatrix} -1-\alpha_1 g_1 & 0 & 0 & \cdots & \alpha_1 g_1 \\ 0 & -\gamma_2 - \alpha_2 g_2 & 0 & \cdots & \alpha_2 g_2 \\ 0 & 0 & -\gamma_3 - \alpha_3 g_3 & \cdots & \alpha_3 g_3 \\ \vdots & \vdots & \vdots & \ddots & \vdots \\ g_1 & g_2 & g_3 & \cdots & -\gamma_S - \sum_{i=1}^n g_i \end{bmatrix} \tag{18}$$

$$\text{and } \mathbf{b}^{NS}_{branch} = \begin{bmatrix} I_1 \\ \gamma_2\beta_2 + I_2 \\ \vdots \\ \gamma_S\beta_S + I_S \end{bmatrix}$$

And for the "chain" model, we have:

$$A^{NS}_{chain} = \begin{bmatrix} -1-\alpha_1 g_1 - \alpha_1 g_2 & \alpha_1 g_2 & 0 & \cdots & \alpha_1 g_1 \\ \alpha_2 g_2 & -\gamma_2 - \alpha_2 g_2 - \alpha_2 g_3 & \alpha_2 g_3 & \cdots & 0 \\ 0 & \alpha_3 g_3 & -\gamma_3 - \alpha_3 g_3 - \alpha_3 g_4 & \cdots & 0 \\ \vdots & \vdots & \vdots & \ddots & \vdots \\ g_1 & 0 & 0 & \cdots & -\gamma_S - g_1 \end{bmatrix} \tag{19}$$

$$\text{and } \mathbf{b}^{NS}_{chain} = \begin{bmatrix} I_1 \\ \gamma_2\beta_2 + I_2 \\ \vdots \\ \gamma_S\beta_S + I_S \end{bmatrix}$$

We diagonalize the matrix $A^{NS} = S^{NS}\Lambda^{NS}(S^{NS})^{-1}$ where Λ^{NS} is the Jordan matrix containing the eigenvalues of A^{NS}, and S^{NS} is the matrix with corresponding eigenvectors in each column. So then solution of any first-order linear differential equation is:

$$\mathbf{V}^{NS}(t) = \mathbf{V}_{inf} + S^{NS}\exp\{\Lambda^{NS}t\}(S^{NS})^{-1} \cdot (\mathbf{V}_0 - \mathbf{V}_{inf}) \quad \text{where} \tag{20}$$

$$\mathbf{V}_{inf} = -(A^{NS})^{-1}\mathbf{b} \tag{21}$$

With biologically-realistic values for the parameters, the eigenvalues are negative and real, and so as $t \to \infty$, $\exp\{\Lambda^{NS} t\}$ will approach the zero matrix, and so $\mathbf{V}^{NS}(t)$ will approach $\mathbf{V}_{inf}$.

The non-spiking solution can be expressed as a map that takes $\mathbf{V}^j = [V_1^j, ..., V_n^j, V_S^j]$, which is the vector containing the initial values of the membrane potentials of each compartment, to $\mathbf{V}^{j+\frac{1}{2}} = [V_1^{j+\frac{1}{2}}, ..., V_n^{j+\frac{1}{2}}, V_S^{j+\frac{1}{2}}]$, which is the vector of the membrane potentials at the onset of the next spike.

$$\Phi_{NS} \,:\, \mathbf{V}^j \to \mathbf{V}^{j+\frac{1}{2}} = \mathbf{V}^{NS}(t^*) \tag{22}$$

If the neuron will not spike, then it will simply output $\mathbf{V}_{inf}$. Computing this map involves finding the earliest time t^* at which $V_S \geq V_{thresh}$. The value of t^* can be computed as the solution to the transcendental equation:

$$V_S^{NS}(t^*) = \mathbf{V}_{inf,S} + \sum_{i=0}^{n} [S^{NS} \exp\{\Lambda^{NS} t^*\} (S^{NS})^{-1}]_{n+1,i} \cdot (\mathbf{V}_{0,i} - \mathbf{V}_{inf,i}) = V_{thresh} \tag{23}$$

We compute the solution of this equation numerically.

Spiking solution

Once the neuron is spiking, the system adheres to a different set of first-order linear differential equations. In the spiking system, the vector $\mathbf{b}_S(t)$ is now time-dependent, and both A_S and $\mathbf{b}_S(t)$ have one fewer dimension since the somatic voltage is entirely described by the spike shape $h(t)$. For the "branch" model, we have:

$$\begin{aligned} A_{branch}^S &= \begin{bmatrix} -1-\alpha_1 g_1 & 0 & \cdots & 0 \\ 0 & -\gamma_2 - \alpha_2 g_2 & \cdots & 0 \\ \vdots & \vdots & \ddots & \vdots \\ 0 & 0 & \cdots & -\gamma_n - \alpha_n g_n \end{bmatrix} \\ \text{and } \mathbf{b}_{branch}^S(t) &= \begin{bmatrix} \alpha_1 g_1 h(t) + I_1 \\ \alpha_2 g_2 h(t) + \gamma_2 \beta_2 + I_2 \\ \vdots \\ \alpha_n g_n h(t) + \gamma_n \beta_n + I_n \end{bmatrix} \end{aligned} \tag{24}$$

For the "chain" model, we have:

$$\begin{aligned} A_{chain}^S &= \begin{bmatrix} -1-\alpha_1 g_1 - \alpha_1 g_2 & \alpha_1 g_2 & 0 & \cdots & 0 \\ \alpha_2 g_2 & -\gamma_2 - \alpha_2 g_2 & \alpha_2 g_3 & \cdots & 0 \\ 0 & \alpha_3 g_3 & -\gamma_3 - \alpha_3 g_3 & \cdots & 0 \\ \vdots & \vdots & \vdots & \ddots & \vdots \\ 0 & 0 & 0 & \cdots & -\gamma_n - \alpha_n g_n \end{bmatrix} \\ \text{and } \mathbf{b}_{chain}^S(t) &= \begin{bmatrix} \alpha_1 g_1 h(t) + I_1 \\ \gamma_2 \beta_2 + I_2 \\ \vdots \\ \gamma_n \beta_n + I_n \end{bmatrix} \end{aligned} \tag{25}$$

Notice that A^S is the top-left $n \times n$ submatrix of A^{NS}, and so is exactly the same as A^{NS} with the last row and last column removed. We move the dependency on the somatic voltage into the vector $\mathbf{b}^S(t)$. We

again diagonalize this matrix $A^S = S^S \Lambda^S (S^S)^{-1}$. Notice that for the "branch" model, since A^S is diagonal, $S^S = (S^S)^{-1} = I$ and $\Lambda^S = A^S$. The spiking solution is then:

$$\mathbf{V}^S(t) = S^S \exp\{\Lambda^S (t - T_0)\} \cdot \left((S^S)^{-1} \mathbf{V}(T_0) + \exp\{\Lambda^S T_0\} \int_{T_0}^{t} \exp\{-\Lambda^S s\} (S^S)^{-1} \mathbf{b}^S(s)\, ds \right) \tag{26}$$

The spiking solution can also be expressed as a map that takes $\mathbf{V}^{j+\frac{1}{2}} = [V_1^{j+\frac{1}{2}}, ..., V_n^{j+\frac{1}{2}}]$, the *dendritic* membrane potentials at spike onset, to $\mathbf{V}^{j+1} = [V_1^{j+1}, ..., V_n^{j+1}]$, which is the vector of the membrane potentials at the end of the spike.

$$\Phi_S \,:\, \mathbf{V}^{j+\frac{1}{2}} \to \mathbf{V}^{j+1} = \mathbf{V}^S(T_a) \tag{27}$$

Generalization to arbitrary dendritic topologies

Extending our "chain" and "branch" models, we can represent any multi-compartment neuron with multiple passive connections using our matrix formulation. This generalization will show that our analysis of the general matrix form of our model is extendable to arbitrary dendritic topologies. The coefficient matrix A_{NS} can be decomposed into a sum of matrices:

$$A^{NS} = L + \sum_{i \neq j} 1_{\{i \text{ connected to } j\}} C_{i,j} \tag{28}$$

The first matrix L is a diagonal matrix representing the intrinsic leak current for each compartment where the m-th diagonal element is $-\gamma_m$ for all m and the matrix is zero everywhere else.

$$L = \begin{bmatrix} -1 & 0 & 0 & \cdots & 0 \\ 0 & -\gamma_2 & 0 & \cdots & 0 \\ 0 & 0 & -\gamma_3 & \cdots & 0 \\ \vdots & \vdots & \vdots & \ddots & \cdots \\ 0 & 0 & 0 & \cdots & -\gamma_S \end{bmatrix} \tag{29}$$

The term $1_{\{i \text{ connected to } j\}}$ indicates whether a connection exists between compartment i and compartment j. If such a connection exists, then $1_{\{i \text{ connected to } j\}} = 1$, otherwise $1_{\{i \text{ connected to } j\}} = 0$. The term $C_{i,j}$ is a matrix that represents the additional terms which characterize the transfer of charge across the connection between compartments i and j.

$$C_{i,j} = \begin{bmatrix} \ddots & & & & \\ & -\alpha_i g_k & \cdots & \alpha_i g_k & \\ & \vdots & \ddots & \vdots & \\ & \alpha_j g_k & \cdots & -\alpha_j g_k & \\ & & & & \ddots \end{bmatrix} \tag{30}$$

The element at position (i, i) is $-\alpha_i g_k$, the element at position (j, j) is $-\alpha_j g_k$, the element at position (i, j) is $\alpha_i g_k$, the element at position (j, i) is $\alpha_j g_k$, and the matrix is zero everywhere else, where k represents the unique index of the connection. As a concrete example to better illustrate the decomposition, we show how

A_{NS}^{branch} can be decomposed into L and $C_{i,j}$ where the number of dendrites is 2:

$$A_{branch}^{NS} = \begin{bmatrix} -1-\alpha_1 g_1 & 0 & \alpha_1 g_1 \\ 0 & -\gamma_2-\alpha_2 g_2 & \alpha_2 g_2 \\ g_1 & g_2 & -\gamma_S-g_1-g_2 \end{bmatrix} = L + C_{S,1} + C_{S,2} \text{ where:}$$

$$L = \begin{bmatrix} -1 & 0 & 0 \\ 0 & -\gamma_2 & 0 \\ 0 & 0 & -\gamma_S \end{bmatrix}, C_{S,1} = \begin{bmatrix} -\alpha_1 g_1 & 0 & \alpha_1 g_1 \\ 0 & 0 & 0 \\ 1\cdot g_1 & 0 & -1\cdot g_1 \end{bmatrix}, C_{S,2} = \begin{bmatrix} 0 & 0 & 0 \\ 0 & -\alpha_2 g_2 & \alpha_2 g_2 \\ 0 & 1\cdot g_2 & -1\cdot g_2 \end{bmatrix} \tag{31}$$

Notice that for physically-realistic values for the parameters, the absolute value of the diagonal element in each row of $C_{i,j}$ is equal to the absolute value of the non-diagonal elements. Additionally, since L_{NS} has no zero elements in the diagonal, then A^{NS} must be strictly diagonally dominant. Therefore, A^{NS} is nonsingular, diagonalizable, and the real parts of the eigenvalues are negative [5]. The argument can also be extended to the spiking solution, as A^S is also strictly diagonally-dominant. However, it is possible to pick values of parameters to be zero such that A^{NS} or A^S is not diagonalizable, but in those cases, the dimensionality of the system can be reduced so that the matrix is diagonalizable, such as removing an irrelevant or isolated compartment from the system.

The return map

Using the two maps we defined above, we can define a new map Φ which takes the initial state of the neuron, $\mathbf{V}^j = \mathbf{V}_0$ (where $V_S(0) = V_R$), to the state of the neuron *after* the next spike, $\mathbf{V}^{j+1}$.

$$\Phi = \Phi_S \circ \Phi_{NS} \ : \ \mathbf{V}^j \to \mathbf{V}^{j+1} \tag{32}$$

This map uses the non-spiking map Φ_{NS} to compute the state of the neuron at the onset of the spike t^*. If the neuron does not spike, then Φ returns $\mathbf{V}_{inf}$ without computing Φ_S. Otherwise, we can then apply Φ_S to the resulting dendritic membrane potential and obtain the state of the neuron at the end of the spike. Note that we discard the somatic membrane potential in our overall map since it will always be V_R at the end of every spike. Thus, even though the overall neuron is a $(n+1)$-dimensional system, we reduce the dynamics to an n-dimensional return map.

We can use the return map to determine the critical voltage V^*, where an initial voltage greater than this value will cause the neuron to spike indefinitely. Any initial voltage smaller than V^* will be quiescent, eventually reaching V_{inf} after ceasing spiking. In the multi-compartment setting, V^* is an $n-2$ dimensional curve in the $n-1$ dimensional space as defined by the map. This curve can be computed as the set of points V^* that satisfies the condition:

$$\begin{cases} \frac{dV_S}{dt}\big|_{t=t^*;V_D(0)\in V^*} & = 0 \\ V_S(t^*;V^*) & = V_{th} \end{cases} \tag{33}$$

Where t^* is the time at which the somatic potential reaches threshold. For example, for the branch model, this equation can be written:

$$-\gamma_S(V_S^{branch}(\mathbf{V}_0) - \beta_S) + I_S + g_1(V_{D_1}^{branch}(\mathbf{V}_0) - V_S^{branch}(\mathbf{V}_0)) = 0 \tag{34}$$

Note that $V_S^{branch}(\mathbf{V}_0)$ and $V_1^{branch}(\mathbf{V}_0)$ are functions of $\mathbf{V}_0$. Thus, V^* is computed by finding the values of

$\mathbf{V}_0$ such that the above condition is met, which can be done simultaneously with solving for t^* in equation 23. In our experiments, we compute this value numerically by searching for the point at which t^* changes from a finite value to infinity, which indicates that it has touched the quiescent region in our return map.

Spike shape

We use two spike shapes in our simulations: square and exponential spike shapes. The square spike is defined as:

$$h(t) = H \tag{35}$$

Where H is the maximal membrane potential of the spike.

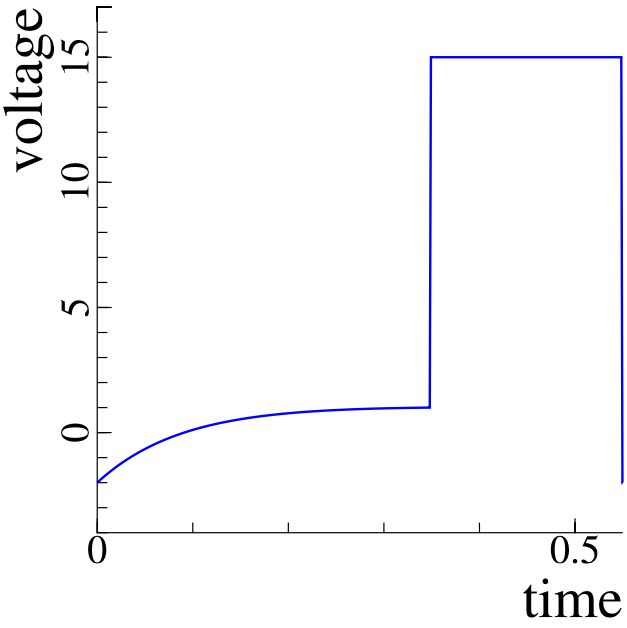

Figure 1: Voltage trace of the square spike shape. The blue curve is the somatic membrane potential, the red curve is that of the first and only dendrite, and the circles indicate our predicted voltages using the maps that we define in the section on non-spiking and spiking solutions. The parameters used to generate this figure were: $\alpha = 1$, $g = 1$, $\beta_S = 1$, $\gamma_S = 10$, $V_R = -2$, $T_a = 0.2$, $I_1 = 0$, and $I_S = -0.6$. The maximal potential of the spike was 15.

The construction of the exponential spike shape is more involved. We parameterize the shape of the spike as a sum of two exponentials:

$$h_p(t) = -\frac{p_b}{p_a - p_d}\exp\{p_d t\} + \left(H + \frac{p_b}{p_a - p_d}\right)\exp\{p_a t\} \tag{36}$$

Where $p_a = 29.5110 \cdot p - 26.7385$, $p_b = -400 \cdot \exp\{-7.377 \cdot p\} - 0.0001$, p_d is solved numerically such that $h(0) = H$ and $h(T_a) = V_R$. The constants used in the expressions for p_a and p_b were set such that the resulting spike shape exhibited afterhyperpolarization and a diverse range of waveforms. The shape of the spike can be controlled with the parameter p, where $p = 0$ has a much thinner spike, and a large subsequent region of afterhyperpolarization. For $p \approx 0.6$, the spike is shaped similarly to a line, connecting $h(0) = H$ to $h(T_a) = V_R$. Finally, when $p = 1$, the spike shape becomes much larger, curving upward and then falling sharply back down to $h(T_a) = V_R$. The voltage traces in Figure 2 show the effect of the spike shape parameter on the spike. This parameterization allows us to continuously explore the effect of a changing spike shape with and without afterhyperpolarization, including a spike shape very similar to the square spike.

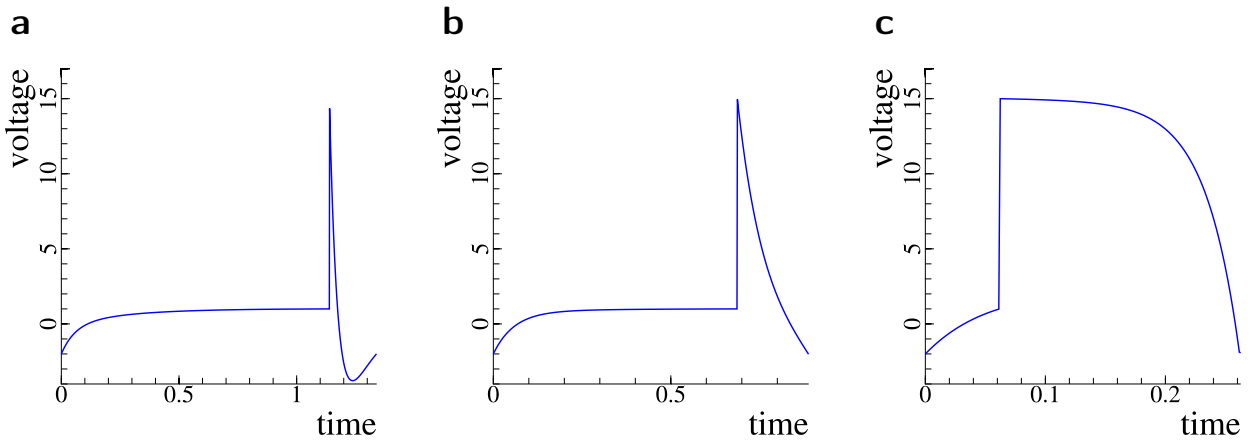

Figure 2: Somatic voltage traces with exponential spike shape parameters $p = 0.05$ for **a**, $p = 0.44972$ for **b**, and $p = 0.90366$ for **c**. Note that the firing frequency increases with p, which we explore in later sections. The other parameters used to generate these figures were: $\alpha = 1$, $g = 5$, $\beta_S = 1$, $\gamma_S = 10$, $V_R = -2$, $T_a = 0.2$, $I_1 = 0$, and $I_S = 1$. The maximal potential of the spike was 15.

Results

Return map analysis

The return map enables us to explore the firing dynamics of the model. We characterize the firing state of the neuron into three classes: the quiescent, monostable, and bistable firing regimes. In the quiescent state, no matter how high the initial membrane potentials are, the neuron will eventually stop firing. Similarly, in the monostable state, no matter what the initial conditions of the neuron, the neuron will not stop spiking. There is a threshold current for which any injected current higher than this value will always put the neuron in the monostable state. This corresponds to the threshold at which the somatic element of $\mathbf{V}_{inf} = -(A^{NS})^{-1}\mathbf{b}$ exceeds the threshold potential V_{th}:

$$V_{inf,S} = -\left[(A^{NS})^{-1} \cdot \mathbf{b}\right]_{n+1} = -\left[(A^{NS})^{-1}\right]_{n+1,n+1} b_{n+1}(I_S) - \sum_{i=1}^{n} \left[(A^{NS})^{-1}\right]_{n+1,i} b_i = V_{th} \tag{37}$$

Here, $\left[(A^{NS})^{-1}\right]_{n+1,i}$ is the element of the matrix $(A^{NS})^{-1}$ in the row $n+1$ and column i, b_i is the i-th element of the vector $\mathbf{b}$. Note that only the term $b_{n+1}(I_S)$ is a function of the injected somatic current I_S and is the only term that depends on I_S in our model. Thus, we can compute the inverse of the function $b_{n+1}(I_S)$, call it $b_{n+1}^{-1}(\cdot)$, and solve for the threshold injected somatic current above which the neuron is monostable:

$$I_{S,th} = b_{n+1}^{-1}\left(\frac{V_{th} + \sum_{i=1}^{n}\left[(A^{NS})^{-1}\right]_{n+1,i} b_i}{[A^{NS}]_{n+1,n+1}}\right) \tag{38}$$

As an example, we compute the threshold somatic current for the "branch" model with two dendrites:

$$I_{S,th} = \frac{V_{th}B}{(\alpha_1 g_1 + 1)(\gamma_2 + \alpha_2 g_2)} - \frac{I_1 g_1}{\alpha_1 g_1 + 1} - \frac{g_2(I_2 + \beta_2\gamma_2)}{\gamma_2 + \alpha_2 g_2} - \beta_S\gamma_S \tag{39}$$

Where $B = g_1\gamma_2 + g_2\gamma_2 + \gamma_2\gamma_S + \alpha_2 g_1 g_2 + \alpha_2 g_2\gamma_S + \alpha_1 g_1 g_2\gamma_2 + \alpha_1 g_1\gamma_2\gamma_S + \alpha_1\alpha_2 g_1 g_2\gamma_S$.

Notice that this threshold current does not depend on the spike shape, which implies that the spike shape does not affect whether the neuron is in the monostable regime.

The return map enables the easy characterization of the excitability of the neuron. Bistability in the two-compartment model resulted from the *ping-pong effect*, where the dendritic compartments are depolarized sufficiently from the previous spike that the resulting flow of current back into the soma would elicit periodic spiking, despite the cell not being in the monostable regime [23]. The voltage trace in Figure 3 is of a neuron in the bistable regime.

The vector plot in Figure 4 visualizes the magnitude and direction of the next iteration of the return map for each initial setting of dendritic voltages. Note that the initial somatic voltage is fixed to $V_R = -2$. The red curve is the V_1-nullcline and the blue curve is the V_2-nullcline, which can be computed by solving the equations $\frac{dV_1}{dt} = 0$ for V_{D_2} and $\frac{dV_2}{dt} = 0$ for V_{D_1}, respectively. The dotted orange line is V^* as described by Equations 36 and 37.

Three plots are shown with different values of injected somatic current. From these plots, it is evident that there exists a range of values for the injected somatic current for which the "branch" model exhibits bistable behavior. This corresponds to the plot where two stable fixed points at the intersections of the nullclines are visible, each corresponding to the quiescent state and to the stable limit cycle in which the neuron repeatedly and regularly spikes. The position of the fixed point corresponding to the quiescent state is identical to $\mathbf{V}_{inf}$. Any value of the injected current greater than this range will exhibit monostable firing. Any value lower than this range will stop firing and be quiescent. In fact, for both models, there are parameter ranges where the neuron can be quiescent, bistable, or monostable.

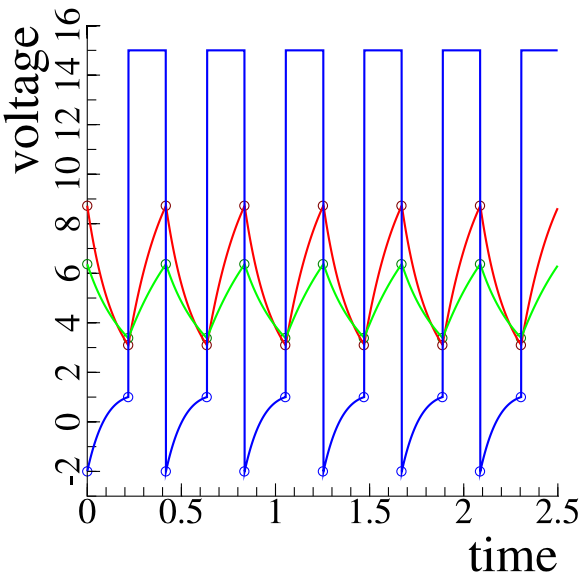

Figure 3: The voltage trace of the stable limit cycle in a three-compartment branch model where $\alpha_1 = 1$, $\alpha_2 = 1$, $g_1 = g_2 = 2$, $\gamma_2 = \gamma_S = 1$, $\beta_2 = \beta_S = 0$, $I_1 = I_2 = 0$, $I_S = -5.6$, $V_R = -2$, $T_a = 0.2$, and a square spike shape with maximal potential 15. The blue curve is the voltage of the soma, red is the voltage of the first dendrite, and green is the voltage of the second dendrite. The curves were generated using a simple Euler loop simulating the system. The circles indicate the values of the solution as predicted by the non-spiking and spiking portions of return map.

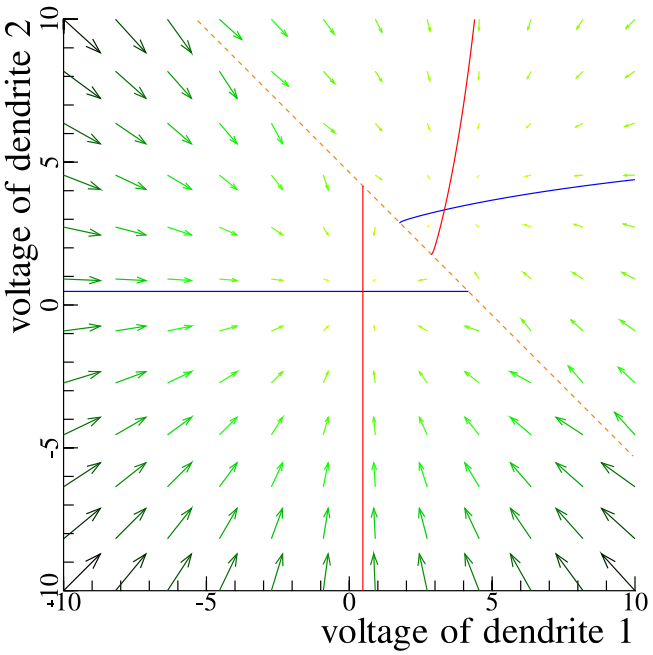

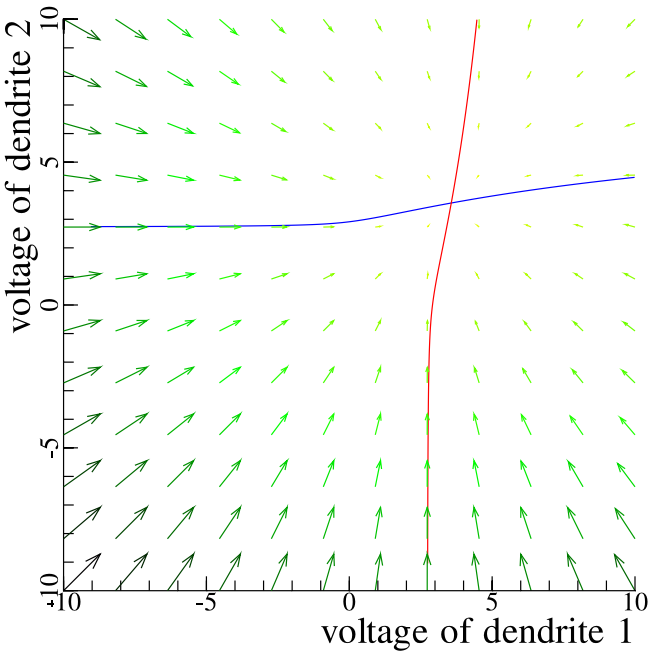

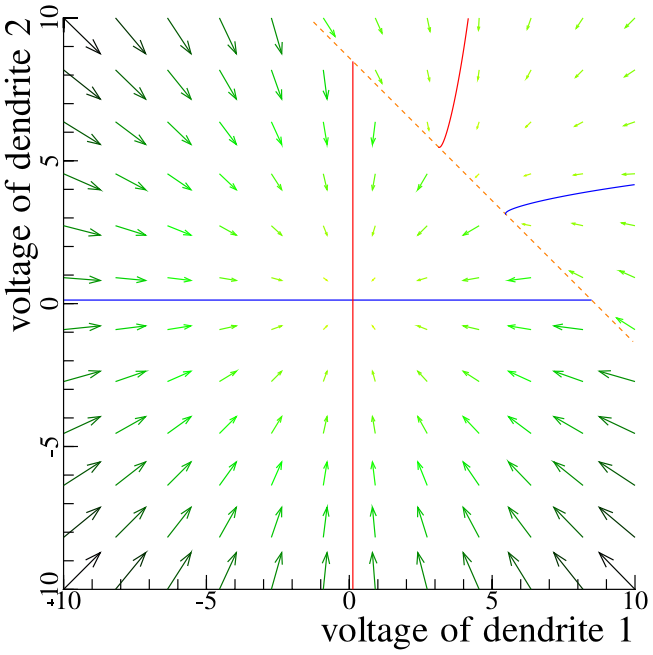

Figure 4: A vector plot representation of the return map where the arrows indicate the direction and relative magnitude of the next iteration of the map. Here the number of dendrites is $n = 2$, and the other parameters: $\alpha_1 = \alpha_2 = 1$, $g_1 = g_2 = 1$, $\beta_2 = \beta_S = 0$, $\gamma_2 = \gamma_S = 1$, $I_1 = I_2 = 0$, $I_S = 0.5$ (left), $I_S = 1.9$ (bottom-left), and $I_S = 2.5$ (bottom-right). As the current is increased, we see the neuron switches from the quiescent state (left) into a bistable regime (bottom-left), and finally, monostability (bottom-right). We are using the "branch" model with the square spike shape ($H = 15$). The red curve is the V_1-nullcline and the blue curve is the V_2-nullcline. The dotted orange curve separates the spiking region from the quiescent region.

Effect of spike shape on firing dynamics

Using our framework, we can determine whether a given parameter set will result in quiescent, monostable, or bistable behavior in the three-compartment neuron (either with a chain or branch topology). We explore the effect of varying the spike shape parameter p for the exponential spike on the firing dynamics. Figure 5a is a bifurcation diagram for the applied somatic current I_S versus the spike shape parameter p. We notice

that when the shape of the spike is too narrow, it becomes more difficult to find parameter ranges with bistability in the system. Only when the spike shape is sufficiently large so that a large amount of current can flow into the dendrites to facilitate the ping-pong effect does bistability appear. Note the effect on the frequency of the stable limit cycle: as the spike shape parameter increases, the spiking frequency increases monotonically. In our model, we observe that afterhyperpolarization during the spike limits the current that can flow from the soma to the dendrites. This will limit the current flowing back from the dendrites into the soma, which in turn inhibits bistability. This is precisely the reason why for low values of the spike shape parameter p in Figure 5a, there is no bistability. Increasing the spike height results in an increase in current flowing into the dendrites, directly increasing the ping-pong effect. Since bistability only occurs prevalently for wider spikes, we will restrict our focus to the square spike.

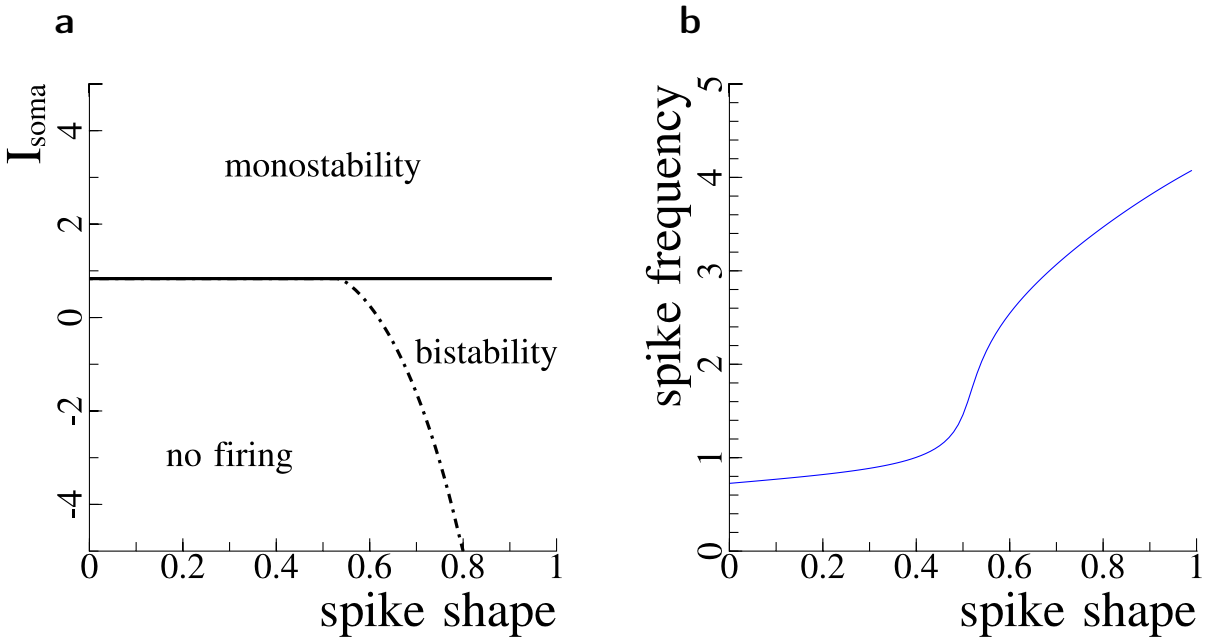

Figure 5: **a:** A bifurcation diagram exploring the effect of the spike shape parameter on the stability of the two-compartment system. **b:** A plot of spike frequency as a function of the spike shape parameter where the injected somatic current I_S is fixed to 1. This is the same value that we use in our later analysis of the effect of spike shape on synchronization properties of the neuron. The parameters used to generate this figure were: $\alpha_1 = \alpha_2 = 1$, $g_1 = g_2 = 1$, $\beta_2 = \beta_S = 0$, $\gamma_2 = \gamma_S = 1$, $I_1 = I_2 = 0$, and $I_S = 1.9$. The square spike shape was used with maximal potential $H = 15$.

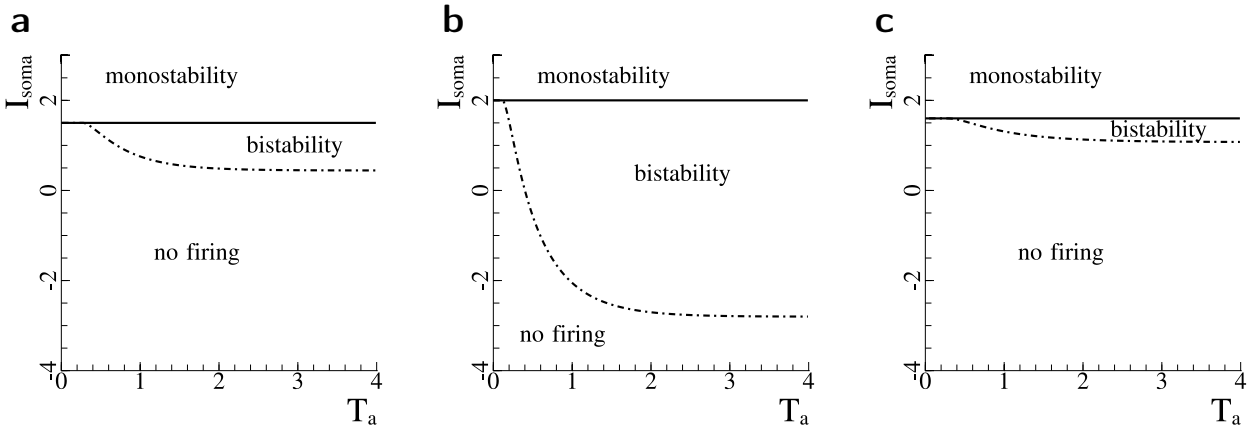

Figure 6: Bifurcation diagrams showing differences in stability with varying the spike duration T_a between the two-compartment model (**a**), the three-compartment branch model (**b**), and the three-compartment chain model (**c**). The parameters used to produce these figures are $\alpha_1 = \alpha_2 = 1$, $g_1 = g_2 = 1$, $\gamma_2 = \gamma_S = 1$, $\beta_2 = \beta_S = 0$, $I_1 = I_2 = 0$, $V_R = -2$, and a square spike shape (with maximal potential $H = 15$).

Figure 6 displays a bifurcation diagrams of the applied somatic current I_S versus the spike duration T_a. We see in all of the dendrite topologies we tested, if the spike duration is too small, there is no range of injected somatic currents for which the neurons are bistable. Comparing Figure 6b to 6a, we see that the addition of the second dendrite in the "branch" configuration dramatically increases the width of the bistable region, and enables bistability for smaller values of the spike duration T_a. This is due to the fact current can flow between the soma and two dendritic compartments. The depolarization of two dendritic compartments provide an additive effect to the current flowing back into the soma. Hence, when the soma stops spiking, current from the dendrites flow back into the soma. When the second dendrite is attached to the soma, we see a double ping-pong effect, where depolarizing current can now flow from two sources into the soma. However, we can see in Figure 6c that if the second dendrite is connected to the first dendrite, as in the "chain" topology, the second dendrite behaves as a sink, drawing current away from the first dendrite, and ultimately, from the soma. This reduces the ping-pong effect, and therefore, the width of the bistable region.

Effect of biophysical parameters on firing dynamics

Figure 7 presents three two-parameter bifurcation diagrams of the injected somatic current I_S versus α_1, the ratio of the somatic surface area to that of the first dendrite. We notice in Figure 7a that when we vary α in the two-compartment model, there is a region of bistability which appears and quickly increases in size as α_1 is raised from 0. The width of this bistable region peaks at around $\alpha_1 \approx 2$, and then contracts in size, disappearing at around $\alpha_1 \approx 8$. In Figure 7b, when another compartment was added, connected to the soma (as in the branch model), the width of the region of bistability increases dramatically. Taking the limit as $\alpha_1 \to \infty$, we notice that the neuron approaches the two-compartment model in Figure 7a where the size parameter of the only dendrite is set to 1. In Figure 7c, we notice that if the extra compartment is instead attached to the first dendrite, the region of bistability is much smaller. Contrasting with the two-compartment case, note that the width of the bistable region does not go to zero as α_1 becomes large. In fact, as α_1 increases, the potential of the first dendrite V_1 approaches $\frac{g_1 V_S + g_2 V_2}{g_1 + g_2}$, which is the weighted average of V_S and V_2, resulting in a coupling between the second dendrite and the soma that is distinct from that in the two-compartment and chain model scenarios. The equivalent two-compartment model has

a new coupling conductance $g = \frac{g_1 g_2}{g_1+g_2} = \frac{1}{2}$, and other parameters: $\alpha = 1$, $\gamma_D = 1$, $\gamma_S = 10$, $\beta_D = \beta_S = 0$, $I_D = 0$, and the square spike shape has height $H = 10$. This equivalent parameter setting is not depicted in any of our figures. Also note that the value of α_1 that maximizes the region of bistability is near not 1, which is a heterogeneous setting for the size parameters of the two dendrites α_1 and α_2. Thus, for many parameter combinations, heterogeneity in the properties of the dendrites can enhance the bistability of the system, even if all of the other parameters are homogeneous. Similarly, there are parameter ranges where the homogeneous settings of the parameters α_1 and α_2 maximize bistability.

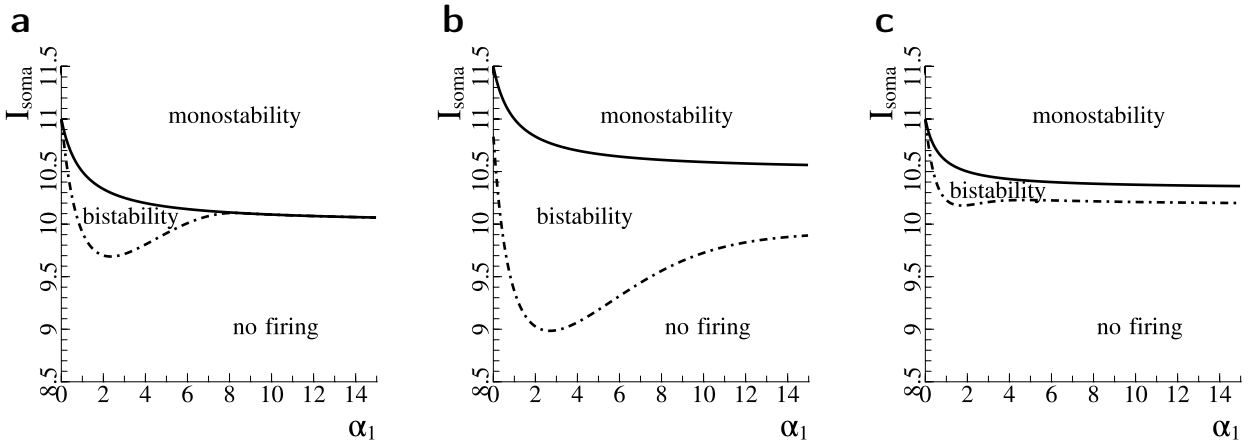

Figure 7: Bifurcation diagrams showing differences in stability with varying α_1, the ratio of the somatic area to the surface area of the first compartment, between the two-compartment model, the three-compartment branch model, and the three-compartment chain model, respectively, from left to right. The solid line is $I_{S,th}$, the threshold injected current such that any higher current will result in the neuron always spiking periodically, as described by Equation 34. The dash-dotted line minimum somatic injected current needed to sustain oscillations, and any smaller value will result in the neuron becoming quiescent. The parameters used to produce these figures are $\alpha_2 = 1$, $g_1 = g_2 = 1$, $\gamma_2 = 1$, $\gamma_S = 10$, $\beta_2 = \beta_S = 0$, $I_1 = I_2 = 0$, $V_R = -2$, $T_a = 0.2$, and a square spike shape (with maximal potential $H = 10$).

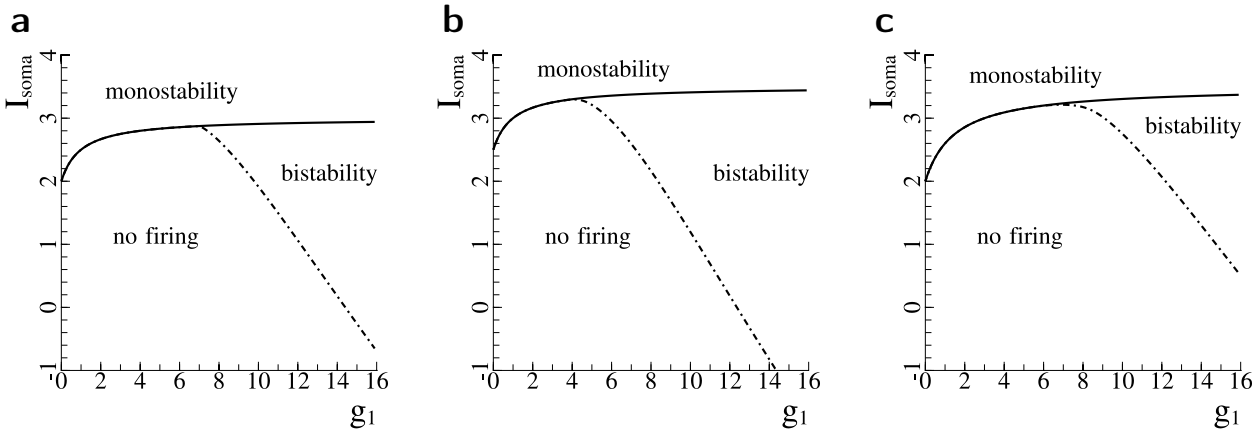

Figure 8: Bifurcation diagrams showing differences in stability with varying g_1, the normalized conductance parameter of the coupling between the soma and first compartment, between the two-compartment model, the three-compartment branch model, and the three-compartment chain model, respectively, from left to right. The parameters used to produce these figures are $\alpha_1 = \alpha_2 = 1$, $g_2 = 1$, $\gamma_2 = 1$, $\gamma_S = 2$, $\beta_2 = \beta_S = 0$, $I_1 = I_2 = 0$, $V_R = -2$, $T_a = 0.2$, and a square spike shape (with maximal potential $H = 5$).

Figure 8 provides three two-parameter bifurcation diagrams, but with respect to the gap junction conductance parameter of the electrical coupling between the soma and the first dendrite g_1. As with varying the ratio of the somatic surface area to that of the first compartment α_1, we see similar differences in behavior between the three models when we vary the coupling conductance g_1. In Figure 8a, it is evident that increasing g_1 directly increases the ping-pong effect, as more current flows between the dendrite and the soma in an additive effect, thereby increasing the width of the bistable region. Note in Figure 8b that the size of the bistable region increases when the second dendritic compartment is connected to the soma as in the branch model. The additional source of depolarizing current enhances the ping-pong effect, seemingly translating the onset of bistability to the left. The width of the bistable region decreases when the compartment is connected to the first dendrite as in the chain model as is evident in Figure 8c. The current that would normally flow from the first dendrite to the soma is now split between the soma and the second dendrite. Acting as a sink, the additional compartment reduces the ping-pong effect, which decreases with width of the bistable region.

Figure 9 further underscores the differences between the three models when the normalized leakage conductance parameter γ_S is varied, and α_1 and g_1 are fixed to 1. Recall that γ_S is a measure of how slowly the somatic potential changes with respect to the first dendrite. Higher values of γ_S enables additional depolarizing current to flow into the soma, enhancing the ping-pong effect. Similar to the earlier cases, the size of the bistable region increases when the second dendritic compartment is connected to the soma as in the branch model, and decreases when the compartment is connected to the first dendrite as in the chain model. For the branch model, the bistable region exists even as γ_S approaches zero, in contrast to both the two-compartment model and the three-compartment chain model.

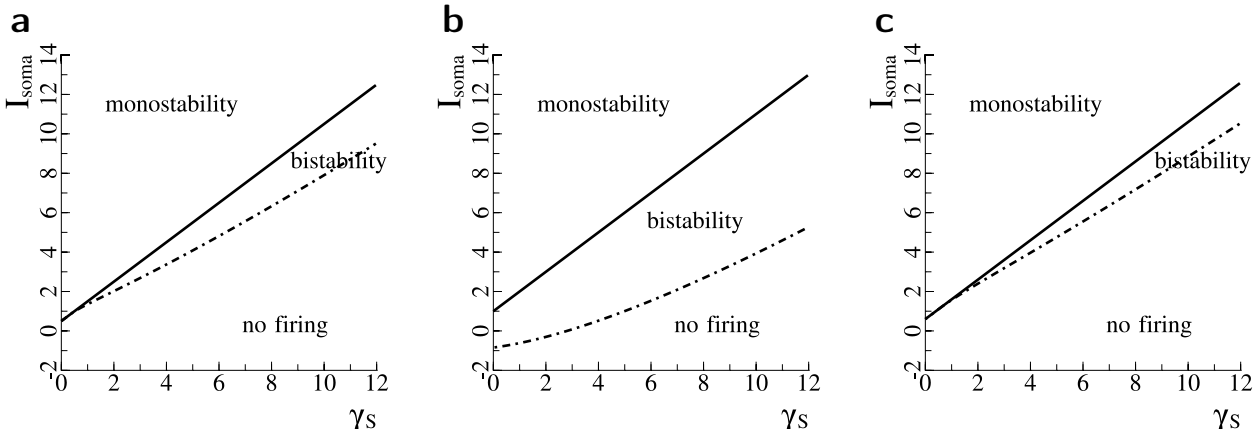

Figure 9: Bifurcation diagrams showing differences in stability with varying γ_1, the normalized leakage conductance, between the two-compartment model, the three-compartment branch model, and the three-compartment chain model, respectively, from left to right. The parameters used to produce these figures are $\alpha_1 = \alpha_2 = 1$, $g_1 = g_2 = 1$, $\gamma_2 = 1$, $\beta_2 = \beta_S = 0$, $I_1 = I_2 = 0$, $V_R = -2$, $T_a = 0.2$, and a square spike shape (with maximal potential $H = 25$).

In Figure 10, we experiment with varying the parameter coupling conductance parameter g_1. In the two-compartment model, the region of bistability grows monotonically with increasing g_1, as is evident in Figure 8, and this behavior was easy to reproduce with the three-compartment model. However, when the value of the ratio of the surface area of the soma to that of the first dendrite α_1 was set to 5.5, and the values of the normalized leakage conductances γ_1 and γ_S are set to 8, we found that even in the two-compartment model, the stability profile of the neuron was changed so that the width of the bistable region no longer

monotonically increases in size. Instead, there is an optimal parameter setting of g_1 that would maximize the size of the bistable region. In the three compartment model, the width of the bistable region further increases and does not go to zero as $g_1 \to \infty$. The addition of a dendrite, depending on the topology of a neuron, can add greater degrees of freedom to the leaky integrate and fire neuron, allowing the model to exhibit a greater variety of firing dynamics profiles.

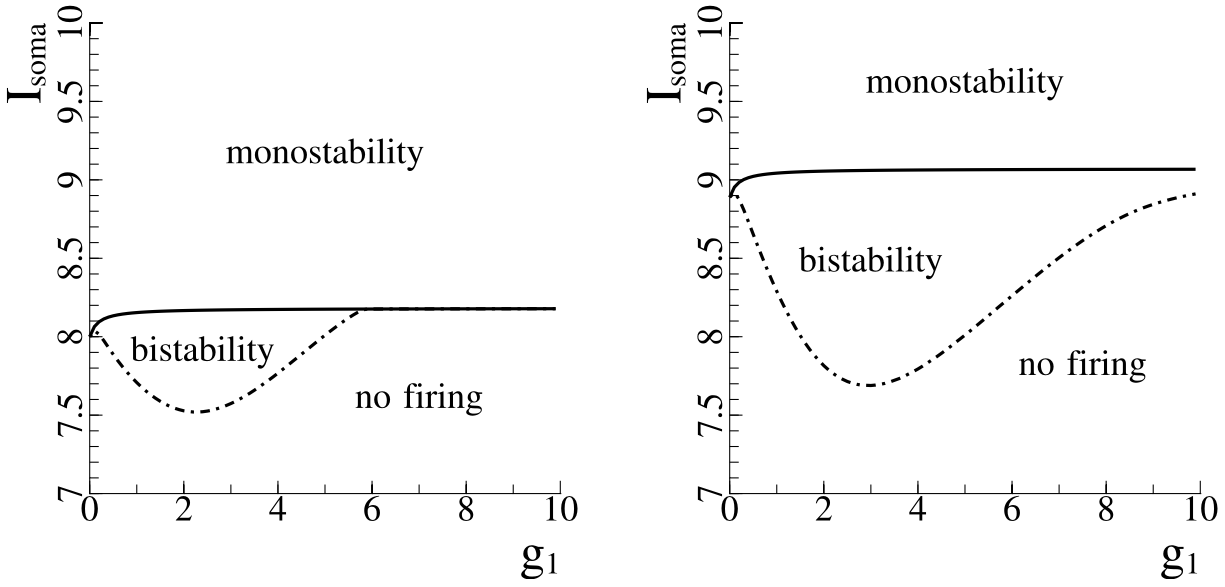

Figure 10: Bifurcation diagrams with varying g_1, the normalized conductance of the coupling between the soma and first dendrite, but with the parameter set: $\alpha_1 = 5.5$, $\alpha_2 = 1$, $g_1 = g_2 = 1$, $\gamma_2 = \gamma_S = 8$, $\beta_1 = \beta_2 = \beta_S = 0$, $I_1 = I_2 = 0$, $V_R = -2$, $T_a = 0.2$, and a square spike shape with maximal potential 15. The left image, however, has the second dendrite removed, whereas the right image has it attached to the soma.

Synchronization properties of LIF neurons with dendritic structure

In this section, we will explore the effect of varying the spike shape on the synchronization dynamics of coupled LIF neurons, where each neuron, when isolated, is in the monostable firing regime. The approach we undertake is valid under any type of coupling between the neurons, as long as the coupling is weak. As an example, we assume that two multi-compartment LIF neurons are coupled via an electrical gap junction at their dendrites, which is ubiquitous among inhibitory interneurons in the neocortex [1]. Thus, our system of linear differential equations is modified with the addition of a term $\alpha_i g_{gap}(V_i^{(2)} - V_i^{(1)})$ that captures the flow of current across the gap junction connecting the two neurons. We let k be the index of the only dendrite at which the electrical coupling between the two neurons exists.

$$\frac{dV_k^{(1)}}{dt} = \sum_{j=1}^{n+1} A_{k,j}^{NS} V_j^{(1)} + b_k^{NS} - \alpha_k g_{gap}(V_k^{(2)} - V_k^{(1)}) \qquad \text{if the neuron is not spiking} \tag{40}$$

$$\frac{dV_k^{(1)}}{dt} = \sum_{j=1}^{n} A_{k,j}^{S} V_j^{(1)} + b_k^{S}(t) - \alpha_k g_{gap}(V_k^{(2)} - V_k^{(1)}) \qquad \text{if the neuron is spiking} \tag{41}$$

The system is defined similarly for the other neuron $V_k^{(2)}$, and the equations for the other compartments are as in our original model. Let ε be the coupling strength coefficient $\alpha_i g_{gap}$ which we can write in dimensional terms as $\varepsilon = \bar{g}_{gap}/(A_i g_{LD_1})$. Note that perturbations as a result of this coupling will be weak if ε is small. We define the non-dimensional period of the limit cycle of each neuron when isolated is T.

Theory of weakly-coupled oscillators

The theory of weakly-coupled oscillators is frequently used to explore the dynamics of oscillating systems of interconnected neurons [24, 21, 8]. In a network of firing neurons, each exhibiting a T-periodic limit cycle when isolated, the state of each neuron can be captured by its phase in its T-periodic limit cycle: $\theta_j(t) = t + \phi_j(t) \in [0, 1)$ where $\phi_j(t)$ is the relative phase of the j^{th} neuron. The reduces the complexity of analysis, as the behavior of each high-dimensional oscillator can be captured by a single-dimensional representation. A system of two coupled neurons can be further simplified by studying the evolution of the phase difference between the two neurons $\phi = \theta_k - \theta_j = \phi_k - \phi_j$.

The evolution of the j^{th} neuronal oscillator's relative phase is governed by the phase equation:

$$\frac{d\phi_j}{dt} = \varepsilon \frac{1}{T} \int_0^T Z_D(t + T\phi_j) I_{coupled}(\phi_k, \phi_j) dt \tag{42}$$

Phase model in the electrically-coupled LIF model

We approximate $I_{coupled}(\phi_k, \phi_j)$ as the difference in voltage between the two compartments in addition to a phase shift: $V_{LC,D}(s + T(\phi_k - \phi_j)) - V_{LC,D}(s)$. This is valid due to our assumption that the coupling between the neurons is weak. Therefore, the membrane potential of the compartments of each neuron will be very strongly attracted to the limit cycle. It is tractable to compute $Z_D(\cdot)$ and $V_D(\cdot)$ since we have the analytic solution for our system.

$$\begin{aligned} \frac{d\phi_j}{dt} &= \varepsilon \frac{1}{T} \int_0^T Z_D(t + T\phi_j) \left(V_{LC,D}(t + T\phi_k) - V_{LC,D}(t + T\phi_j) \right) dt \\ &= \varepsilon \frac{1}{T} \int_0^T Z_D(s) \left(V_{LC,D}(s + T(\phi_k - \phi_j)) - V_{LC,D}(s) \right) ds \text{ where } \varepsilon \text{ is the coupling strength.} \\ &= H(T(\phi_k - \phi_j)) \end{aligned} \tag{43}$$

Where $H(T(\phi_k - \phi_j))$ is called the H-function or interaction function and describes the modulation of the j^{th} oscillator's instantaneous frequency resulting from the coupling current, which in our case is the passive current flow between dendritic compartments $V_{LC,D}(T(t + \phi_k)) - V_{LC,D}(T(t + \phi_j))$. The infinitesimal phase response curve, or *iPRC*, $Z_D(s)$ describes the change in the phase of an oscillator in response to an δ-function stimulus at the point s in the limit cycle of the oscillator. The iPRC can be computed by perturbing the isolated neuron with a small current pulse at different points along the limit cycle, and measuring the resulting change in phase. An alternative approach to compute the iPRC is to find the solution to the adjoint problem of the oscillating system linearized around its limit cycle [24].

Deriving the iPRC

We will now derive the iPRC for the multi-compartment LIF model by solving the corresponding adjoint problem. Recall that the membrane potentials of the compartments of our neuron model are characterized

by the piecewise differential system: $\frac{d\mathbf{V}}{dt} = A^{NS}\mathbf{V} + \mathbf{b}^{NS}$ when not spiking, and $\frac{d\mathbf{V}}{dt} = A^{S}\mathbf{V} + \mathbf{b}^{S}(t)$ once V_S reaches threshold. These can be expressed as $\frac{d\mathbf{V}}{dt} = \mathbf{F}(\mathbf{V})$ where $\mathbf{F}$ is a piecewise vector-valued function. Suppose that a solution exists with a stable limit cycle. We derive the iPRC by solving for $\mathbf{Z}(t)$ in the adjoint equation [24]:

$$\frac{d\mathbf{Z}}{dt} = -D[\mathbf{F}(\mathbf{V}_{LC}(t))]^{\top}\mathbf{Z} \tag{44}$$

Where D is the Jacobian matrix and $\mathbf{V}_{LC}(t)$ is a vector of the membrane potentials at each compartment, representing the solution at the stable limit cycle evaluated at t. This iPRC specifies how the system will react to an infinitesimal pulse of current into any of the compartments (each compartment has an iPRC, corresponding to the response of the oscillator to a current impulse within that compartment). Notice that the Jacobian is taken with respect to the membrane potentials, and so $D[\mathbf{F}(\mathbf{V}_{LC}(t))]^{\top}$ is equivalent to $A_{NS}^{\top}$ when the neuron is not spiking. When spiking, however, $D[\mathbf{F}(\mathbf{V}_{LC}(t))]^{\top}$ is the matrix where the top-left $(n-1)\times(n-1)$ block is $A_S^{\top}$ and all other elements are zero where n is the total number of compartments. Thus, the iPRC for all compartments is simply the solution to $\frac{d\mathbf{Z}}{dt} = -A_{NS}^{\top}\mathbf{Z}$ when not spiking, and for the dendritic compartments only, the iPRC is the solution to $\frac{d\mathbf{Z}}{dt} = -A_S^{\top}\mathbf{Z}$ (the somatic iPRC is the solution to $\frac{dZ_S}{dt} = 0$). Since we can diagonalize $A_{NS} = S_{NS}\Lambda_{NS}S_{NS}^{-1}$, then it must be the case that $-A_{NS}^{\top} = (S_{NS}^{\top})^{-1}(-\Lambda_{NS})S_{NS}^{\top}$. So when the neuron is not spiking, we can write the general solution to $\mathbf{Z}(t)$:

$$\mathbf{Z}(t) = (S_{NS}^{\top})^{-1}e^{-\Lambda_{NS}t}S_{NS}^{\top}\cdot\mathbf{Z}_0 \tag{45}$$

When spiking however, we know that $A_S = S_S\Lambda_S S_S^{-1}$ is similarly diagonalizable, and so:

$$\mathbf{Z}(t) = (S_S^{\top})^{-1}e^{-\Lambda_S t}S_S^{\top}\cdot\mathbf{Z}(t^*) \tag{46}$$

Where $t\in[t^*, t^*+T_a)$, t^* is the time at which V_S hits the threshold voltage. Note that the somatic iPRC $Z_S(t) = 0$ is constant during the spiking phase since no amount of current will change the shape of the spike.

To determine the values of the integration constants $\mathbf{Z}_0$, $\mathbf{Z}(t^*)$, and $Z_{S,0}$, we apply the normalization condition: $\mathbf{Z}(t)\cdot\mathbf{F}(\mathbf{V}_{LC}(t)) = 1$ for all t. In the non-spiking condition, we have $\mathbf{Z}(t)\cdot\mathbf{F}(\mathbf{V}_{inf} + S_{NS}e^{\Lambda_{NS}t}S_{NS}^{-1}\cdot(\mathbf{V}_0 - \mathbf{V}_{inf}))$. Simplifying:

$$\begin{aligned}\mathbf{Z}(t)^{\top}\mathbf{F}(\mathbf{V}_{LC}(t)) &= \mathbf{Z}(t)^{\top}(S_{NS}\Lambda_{NS}S_{NS}^{-1}(-S_{NS}\Lambda_{NS}^{-1}S_{NS}^{-1}\mathbf{b} + S_{NS}e^{\Lambda_{NS}t}S_{NS}^{-1}(\mathbf{V}_0 + S_{NS}\Lambda_{NS}^{-1}S_{NS}^{-1}\mathbf{b})) + \mathbf{b})\\ &= \mathbf{Z}_0\cdot(A_{NS}\mathbf{V}_0 + \mathbf{b}) = 1\end{aligned} \tag{47}$$

This indicates that the fact that the normalization condition holds for values of t at which the neuron is not spiking does not provide any additional constrains/information than when the condition is true only at $t = 0$. However, we can enforce the T-periodicity of the system with the following condition: If we know the limit cycle $\mathbf{V}_{LC}(t)$, then we know the time at which the spike begins and the interspike interval of the neuron. Thus, we can simply plug these into the matrix solutions we derived above. However, there is the problem that the spiking portion of the iPRC has one fewer dimension than the non-spiking portion. If t^* is the time of spike onset, and the neuron as n dendrites, then $\mathbf{Z}(t^*) = (S_{NS}^{\top})^{-1}e^{-\Lambda_{NS}t^*}S_{NS}^{\top}\cdot\mathbf{Z}_0$ is an $(n+1)$-dimensional vector representing the value of the iPRC at time t^*, as computed using the non-spiking iPRC solution. Notice that the somatic iPRC is zero when the neuron is firing, and so the iPRC at $t > t^*$ is the n-dimensional vector $\mathbf{Z}(t) = (S_S^{\top})^{-1}e^{-\Lambda_S(t-t_A)}S_S^{\top}\cdot(\mathbf{Z}(t^*))_{1:n}$ where $(\mathbf{Z}(t^*))_{1:n}$ is the first n elements of the iPRC evaluated at t^*. Evaluating $\mathbf{Z}(t)$ at the end of the spike $t^*+T_a = T$, we can impose T-periodicity by setting $\mathbf{Z}(0) = \mathbf{Z}(t^*+T_a)$, and utilizing the constraint that the dendritic iPRCs are continuous. This

gives us an n-dimensional linear system of equations in $\mathbf{Z}_0$, which has $n+1$ unknowns:

$$(\mathbf{Z}_0)_{1:n} = (S_S^\top)^{-1} e^{-\Lambda_S (t-t_A)} S_S^\top \cdot \left((S_{NS}^\top)^{-1} e^{-\Lambda_{NS} t^*} S_{NS}^\top \cdot \mathbf{Z}_0 \right)_{1:n} =: f(\mathbf{Z}_0) \tag{48}$$

Given the limit cycle $\mathbf{V}_{LC}(t)$ and the value of the iPRC at $t=0$, including the value of the somatic iPRC, we can compute $f(\mathbf{Z}_0)$ to find the unique value of the iPRC at $t = t^* + T_a = T$. Similarly, given the value of the iPRC at time $t=T$, we can compute the unique $\mathbf{Z}_0$ such that $\mathbf{Z}(T) = [f(\mathbf{Z}_0), Z_{S,0}]$, and so the space of solutions $\mathbf{Z}_0$ has dimension n. Thus, by adding the normalization condition $\mathbf{Z}_0 \cdot (A_{NS}\mathbf{x}_0 + \mathbf{b}) = 1$, we have a total of $n+1$ equations with $n+1$ unknowns, enabling us to find the unique solution for $\mathbf{Z}_0$.

Notice that the iPRC depends heavily on the parameters governing the A_{NS} and A_S matrices. There is an implicit dependence on both $\mathbf{b}_{NS}$ or $\mathbf{b}_S(t)$, which specify the shape of the spike, for example, since both affect the stable limit cycle $\mathbf{V}_{LC}(t)$, which will influence $\mathbf{Z}_0$ via the normalization condition. But only the A_{NS} and A_S matrices can change the overall shape of the iPRC. In addition, given the properties of A_{NS} and A_S, the iPRC system has a single unstable fixed point at the origin, as all of the eigenvalues have positive real parts. We emphasize that this approach is sufficiently general to compute the iPRC for any multi-compartment LIF neuron. We will showcase an example of how this can be done for the two-compartment model.

Example: Two-compartment model

We present an example of this calculation for the two-compartment model. For the two-compartment model, we have the following linear differential equation for $\mathbf{Z}(t)$:

$$\frac{d\mathbf{Z}}{dt} = \begin{bmatrix} \alpha g + 1 & -g \\ -\alpha g & g + \frac{\tau_D}{\tau_S} \end{bmatrix} \begin{bmatrix} Z_D(t) \\ Z_S(t) \end{bmatrix} = -A_{NS}^\top \cdot \mathbf{Z}(t) \tag{49}$$

We then diagonalize $-A^\top = S^\top(-\Lambda)(S^\top)^{-1}$ and so the solution is as follows:

$$\mathbf{Z}(t) = (S_{NS}^\top)^{-1} e^{-\Lambda_{NS} t} S_{NS}^\top \cdot \mathbf{Z}_0$$

$$\begin{aligned} \lambda_D &= -\tfrac{1}{2}(1 + g + \alpha g + \tfrac{\tau_D}{\tau_S} + R) & \lambda_S &= -\tfrac{1}{2}(1 + g + \alpha g + \tfrac{\tau_D}{\tau_S} - R) \\ S &= \begin{bmatrix} \frac{1}{g} c_D & \frac{1}{g} c_S \\ 1 & 1 \end{bmatrix} & S^{-1} &= \begin{bmatrix} -\frac{g}{R} & \frac{1}{R} c_S \\ \frac{g}{R} & -\frac{1}{R} c_D \end{bmatrix} \end{aligned} \tag{50}$$

Multiplying these terms, we obtain:

$$\mathbf{Z}(t) = \frac{1}{R} \begin{bmatrix} c_S e^{-\lambda_S t} - c_D e^{-\lambda_D t} & c_D (e^{-\lambda_D t} - e^{-\lambda_S t}) \\ -c_S (e^{-\lambda_D t} - e^{-\lambda_S t}) & c_S e^{-\lambda_D t} - c_D e^{-\lambda_S t} \end{bmatrix} \cdot \mathbf{Z}_0 \tag{51}$$

Where $R = \sqrt{\alpha^2 g^2 + 2\alpha g^2 - 2\alpha g \frac{\tau_D}{\tau_S} + 2\alpha g + g^2 + 2g\frac{\tau_D}{\tau_S} - 2g + \frac{\tau_D^2}{\tau_S^2} - 2\frac{\tau_D}{\tau_S} + 1}$. For readability, let $c_D = \lambda_D + g + \frac{\tau_D}{\tau_S}$ and $c_S = \lambda_S + g + \frac{\tau_D}{\tau_S}$. And so if we plug these into the analytic solution, we obtain the following

two equations for the non-spiking portion of the iPRC:

$$\begin{aligned} Z_D(t) = & \quad -\frac{1}{R}e^{-\lambda_D t}(c_D Z_D(0) + g Z_S(0)) + \frac{1}{R}e^{-\lambda_S t}(c_S Z_D(0) + g Z_S(0)) \\ Z_S(t) = & \quad \frac{1}{R}c_S e^{-\lambda_D t}(\frac{1}{g}c_D Z_D(0) + Z_S(0)) - \frac{1}{R}c_D e^{-\lambda_S t}(\frac{1}{g}c_S Z_D(0) + Z_S(0)) \end{aligned} \tag{52}$$

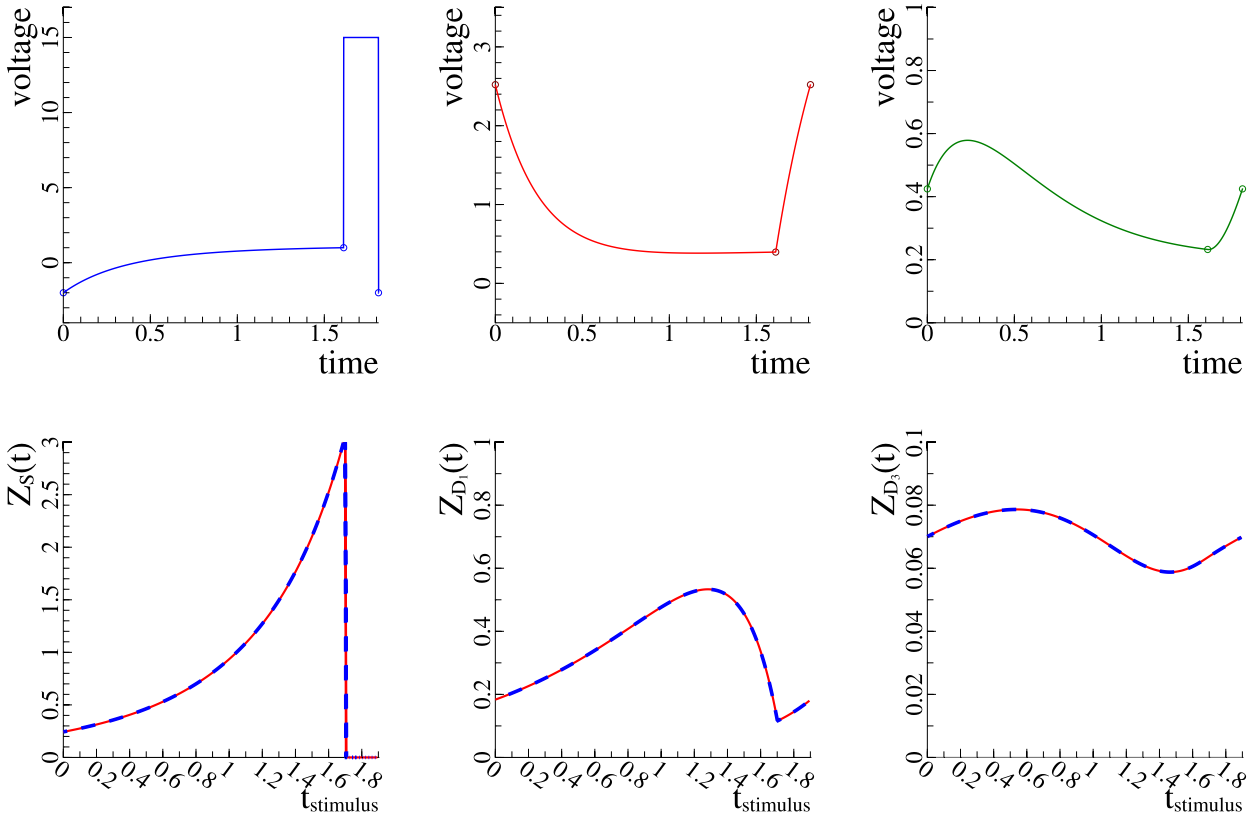

Figure 11: These are plots of the limit cycle (top row) and infinitesimal phase response curves (bottom row) of the soma, first dendrite, and third dendrites, respectively from left to right, of a model neuron where the dendrites are arranged in a linear chain. The blue dotted curve is the simulated iPRC, where a square pulse with magnitude 0.1 and duration 0.001 was delivered to the respective compartment at each time during the limit cycle, and the subsequent deviation from the limit cycle was then measured. The red curve is our analytic solution. Notice the difference in the scaling of the y-axis. The first portion of the curve corresponds to the non-spiking region. The last portion ($T_a = 0.2$) corresponds to the spiking region. Each dendrite in the chain acted as a "filter," smoothing and decreasing the magnitude of the iPRC with each compartment. The parameters used for to generate these figures were: $\alpha_i = 1$, $\beta_i = 0$, $g_i = 1$, and $\gamma_i = 1$ for all compartments i, $I_i = 0$ for all dendrites, $V_R = -2$, $T_a = 0.2$, $I_S = 1.8$, and a square spike shape was used with maximal potential 15.

The spiking portion is simpler since $Z_S(t) = 0$, and so our system is simply $\frac{dZ_D}{dt} = (\alpha g + 1) \cdot Z_D$, and so $Z_D(t) = e^{(\alpha g+1)(t-T+T_a)} Z_D(T - T_a)$ is the iPRC of the spiking portion, where $T - T_a$ is the time of spike onset. To compute the initial conditions, assume we start at time 0 at the onset of the non-spiking region with $Z_D(0)$ and $Z_S(0)$ (we note that neither of these are zero). Then the neuron evolves until the somatic potential reaches threshold, and the neuron begins to spike at time $T - T_a$ (the difference

between the interspike duration and the spike duration). We note that $Z_D(t)$ must be continuous, and so $Z_D(T-T_a) = \frac{1}{R}c_D e^{-\lambda_D(T-T_a)}(Z_D(0) - Z_S(0)) - \frac{1}{R}e^{-\lambda_S(T-T_a)}(c_S Z_D(0) + c_D Z_S(0))$. During spiking, $Z_S(t)$ is zero, and so at time $T - T_a$ and T, there are discontinuities where $Z_S(t)$ jumps down to zero and then back up to $Z_S(0)$. To enforce T-periodicity, we substitute our solution into $Z_D(T) = Z_D(0)$ and we obtain the following relation:

$$Z_D(0) = \frac{1}{R}c_S e^{(\alpha g+1)T_a} e^{-\lambda_D(T-T_a)}(Z_S(0) - Z_D(0)) + \frac{1}{R}e^{(\alpha g+1)T_a} e^{-\lambda_S(T-T_a)}(c_S Z_D(0) - c_D Z_S(0)) \quad (53)$$

Notice that this relation is linear in $Z_D(0)$ and $Z_S(0)$, and so we can apply the normalization condition at time 0 to obtain the another linear relation:

$$1 = ((-\alpha g + 1)V_D(0) + \alpha g V_S(0) + I_D)Z_D(0) + (gV_D(0) + (-g - \gamma_S)V_S(0) + \gamma_S\beta_S + I_S)Z_S(0) \quad (54)$$

Note that V_D and V_S are the voltages of each of the compartments at the beginning of the non-spiking portion of the limit cycle. This gives us a system of two linear equations which we can solve to find the initial values of the iPRC.

Back to the phase model

Let $\phi = \phi_k - \phi_j$ be the phase difference between two multi-compartment LIF oscillators electrically-coupled at their dendrites. The G-function is the description of the evolution of the phase difference:

$$\frac{d\phi}{dt} = H(-\phi) - H(\phi) = G(\phi) \quad (55)$$

Where the H-function is defined in Equation 42. The zeros of the G-function correspond to phase-locked states in this system of coupled neurons. The first derivative test can be used to determine the stability of these phase-locked states [24].

Including heterogeneity in the phase model

The above derivation made the assumption that the coupled neurons were identical. We can incorporate heterogeneity between the neurons by modeling its effect as a difference in the intrinsic firing frequency between the two somata. This results in the following change to the phase difference equation:

$$\frac{d\phi}{dt} = \Delta\omega + G(\phi) \quad (56)$$

Where $\Delta\omega$ is the difference in intrinsic firing frequency between the coupled neurons. Note that the phase-locked states are now given by the intersection of the G-function with the horizontal line $-\Delta\omega$. Let $\Delta\omega^*$ be the value of $\Delta\omega$ such that any greater difference in firing frequency will result in the loss of all phase-locked states. Therefore, $\Delta\omega^*$ is the maximum extent to which a system of two weakly-coupled oscillators can tolerate a difference in firing frequency before losing synchrony [22]. We use this are our definition of robustness, as phase-locked systems with larger values of $\Delta\omega^*$ are more robust to heterogeneity.

$$\text{robustness} = \max_{\phi} \left| \frac{1}{\tau_D} G(\phi) \right| \quad (57)$$

Since frequency here is defined in terms of dimensional time, we must apply a correction to our computation of the H-function using the transformation $t = \bar{t}/\tau_D$. Similarly, we need to ensure that the iPRC is in terms of frequency, and so we divide by T:

$$\frac{d\phi_j}{d\bar{t}} = \varepsilon \frac{1}{\tau_D T} \int_0^T \frac{Z_D(s)}{T} \left(V_D(s + T(\phi_k - \phi_j)) - V_D(s) \right) ds \tag{58}$$

To select the value of the coupling coefficient ε, recall that $\varepsilon = \bar{g}_{gap}/(A_i g_{LD_1}) = \bar{g}_{gap}/(4\pi R_i^2 g_{LD_1})$ where R_i is the radius of compartment i. We select the biophysically-realistic value of $\varepsilon = 0.1$ to use in our experiments.

Results

Effect of spike shape on iPRC

The effect of spike shape on the behavior of the system consisting of two weakly coupled two-compartment neurons is significant. Figure 12 shows that the shape of the iPRC very clearly changes with the changing spike shape. These iPRC curves correspond to the voltage traces of the system in Figure 2. As the spike shape becomes more and more linear, with the afterhyperpolarization being reduced, the magnitude of the iPRC increases. Then, a bifurcation occurs, and we can see by $p = 0.9$, the magnitude of the iPRC is greatly reduced.

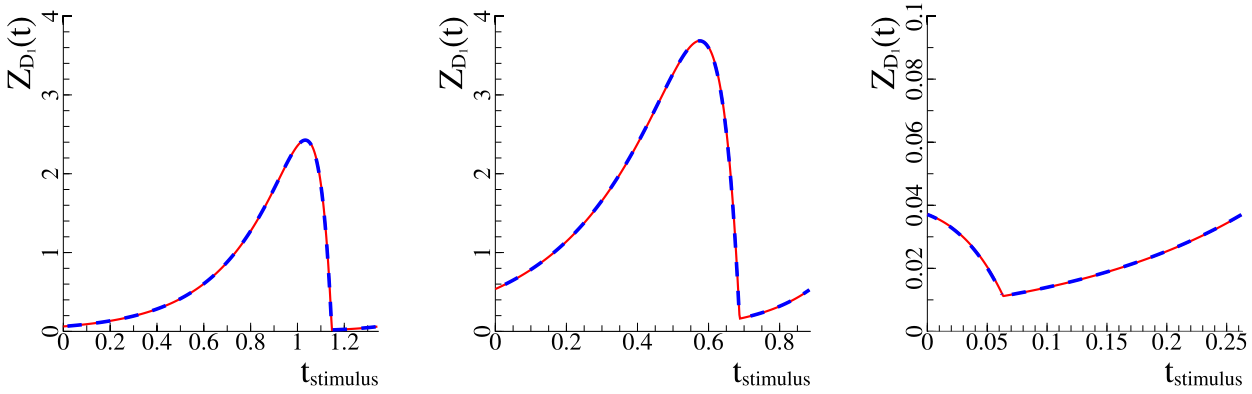

Figure 12: Dendritic iPRC plots with spike shape parameters $p = 0.04$, $p = 0.44972$, and $p = 0.90366$, respectively, from left to right. The blue dotted curve is the simulated iPRC, where a square pulse with magnitude 0.1 and duration 0.001 was delivered to the respective compartment at each time during the limit cycle, and the subsequent deviation from the limit cycle was then measured. The red curve is our analytic solution. Notice the difference in the scaling of the y-axis. The parameters used to generate this figure were: $\alpha_1 = \alpha_2 = 1$, $g_1 = g_2 = 1$, $\beta_2 = \beta_S = 0$, $\gamma_2 = \gamma_S = 1$, $I_1 = I_2 = 0$, and $I_S = 1.9$.

Effect of spike shape on iPRC

A more comprehensive graphical representation of the bifurcations that occur is visible in Figure 13. There are two bifurcations in this system: one at $p \approx 0.2$ and the second at $p \approx 0.5$. When the spike shape parameter is small ($p < 0.2$), there is significant afterhyperpolarization in the system, and we notice that the

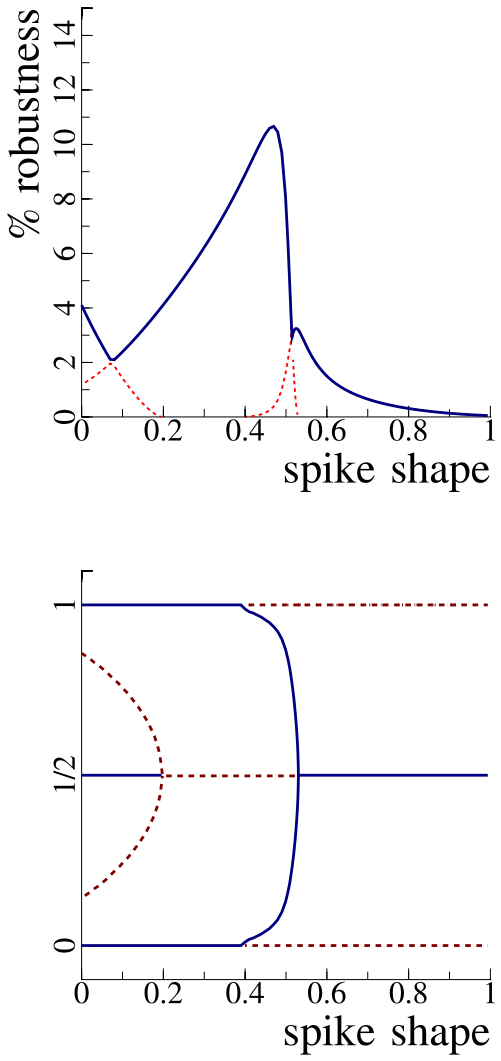

Figure 13: **Top:** Robustness plot, where the blue curve is the maximum absolute value of the G-function, and the red dotted curves indicate the magnitudes of local maxima and minima.
Bottom: Bifurcation diagram of the synchrony properties of the coupled oscillator system as computed from the zeros of the G-function. The solid blue curves indicate stable fixed points, whereas the red dotted lines indicate unstable points. The parameters used to generate this figure were: $\alpha_1 = \alpha_2 = 1$, $g_1 = g_2 = 1$, $\beta_2 = \beta_S = 0$, $\gamma_2 = \gamma_S = 1$, $I_1 = I_2 = 0$, and $I_S = 1.9$.

system of coupled neurons are actually bistable. Depending on the initial conditions of the system, the neurons can either evolve to be synchronously or asynchronously firing. The robustness of this behavior is actually quite high, ranging from 2% to 4%. After this first bifurcation, the asynchronous behavior is no longer stable, and only synchrony exists. The robustness of this synchronous behavior is very high, reaching more than 10% just before the second bifurcation, where it drops off sharply to about 3%.

At this second bifurcation, we see that perfectly synchronous behavior is no longer stable. The fixed point splits and the two points move continuously toward each other (toward asynchrony). This is another region of bistability. This implies that there are settings for parameters for the two-compartment model such that the stable point can be arbitrarily positioned between synchrony and asynchrony. In our other simulations, we were able to "stretch" this bifurcation so that it would not be as sensitive to any of the parameters. After this bifurcation, the system becomes firmly asynchronous. However, the robustness of this asynchrony becomes much lesser, decreasing toward 0% as the spike shape approaches $p = 1$.

In our simulations, we observe that the robustness is very closely related to how close the system is to "not firing," in that a system which will be quiescent with a decrease in injected current is more robust in its synchrony characteristics than a system that will not become quiescent with the same decrease in current. For example, in this experiment, we can see in the corresponding bifurcation diagram in Figure 5 that, along the line $I_S = 1$, the system is very close to the "no firing" region up until $p \approx 0.55$. After this point, the system becomes increasingly distant from the quiescent state (it can tolerate a great loss of injected current, as the stable limit cycle will still exist, even in the bistable regime).

Conclusion

We presented the multi-compartment leaky integrate-and-fire model, enabling the modeling of arbitrarily large trees of dendritic compartments. We showed when the parameters g_i, α_i, γ_i are set to positive, physically-realistic

values, then the matrix representing the differential system of equations can be diagonalized, and all of the eigenvalues have negative real parts, implying that the system will always have a stable fixed point $\mathbf{V}_{inf}$. We provided a parameterization of the spike shape as a sum of two exponentials, which can exhibit after-hyperpolarization. By characterizing the excitability of f-I curves, we studied the effect of spike shape on the firing dynamics of the neuron. We also found that depending on the topology of the dendritic tree, and the biophysical characteristics of each compartment, additional compartments provided the model with increased flexibility in the kinds of behavior that it can exhibit. For example, for some parameters, adding the dendrite to the soma would enhance the ping-pong effect, and therefore, enhance bistability. Whereas adding the dendrite to the first dendrite would act a sink, pulling current away from the first dendrite that would have otherwise gone to the soma where it would facilitate the ping-pong effect. This resulted in lesser bistability. Dendritic properties have a significant effect on the firing dynamics of the multi-compartment LIF neuron.

Next, we utilized the theory of weakly-coupled oscillators to study the synchronization dynamics of two electrically-coupled multi-compartment LIF neurons. We derived the iPRC for the soma and all of the dendrites. As an example, we focused on the two-compartment model, deriving its iPRC, H and G-functions. We explored the effects of spike shape on the stability and synchrony characteristics of the system. We found that thinner spikes, which exhibit afterhyperpolarization, and where less current flows into the dendrites, can elicit bistability between synchrony and asynchrony. When the shape of the spike is wider, the system loses this bistability and exhibits only asynchrony. We notice the similarity of the synchrony properties of our simple two-compartment model to the two-compartment conductance-based model presented in [16], capturing many of the same bifurcations. Although in our case, we varied the spike shape, which has a similar effect as varying the injected current, since increasing the spike shape parameter p would increase the width and height of the spike, increasing the resulting current injected into the dendrites. This suggests that our simplified multi-compartment leaky integrate-and-fire model captures the same synchrony behaviors as the full conductance-based equivalent, even in the two-compartment case. Thus, spike shape plays an instrumental role in affecting the synchronization dynamics of multi-compartment LIF neurons. Further exploration into the capabilities of the multi-compartment LIF model will help develop a better understanding of the purpose of dendrites, electrical coupling, and the role of spike shape.

References

[1] Amitai, Y., Gibson, J., Beierlein, M., Patrick, S., Ho, A., Connors, B., and Golomb, D. The spatial dimensions of electrically coupled networks of interneurons in the neocortex. *J Neurosci 22*, 10 (2002), 4142–52.

[2] Bean, B. P. The action potential in mammalian central neurons. *Nat Rev Neurosci 8*, 6 (2007), 451–65.

[3] Brette, R., and Gerstner, W. Adaptive exponential integrate-and-fire model as an effective description of neuronal activity. *Journal of Neurophysiology 94*, 5 (2005), 3637–3642.

[4] Connors, B. W., and Long, M. A. Electrical synapses in the mammalian brain. *Annual Review of Neuroscience 27*, 1 (2004), 393–418.

[5] Dafchahi, F. Computing of signs of eigenvalues for diagonally dominant matrix for inertia problem. *Appl. Math. Sci., Ruse 2*, 29-32 (2008), 1487–1491.

[6] De Polavieja, G. G., Harsch, A., Kleppe, I., Robinson, H. P. C., and Juusola, M. Stimulus history reliably shapes action potential waveforms of cortical neurons. *Journal of Neuroscience 25*, 23 (2005), 5657–5665.

[7] Deans, M. R., Gibson, J. R., Sellitto, C., Connors, B. W., and Paul, D. L. Synchronous activity of inhibitory networks in neocortex requires electrical synapses containing connexin36. *Neuron 31* (2001), 477–485.

[8] Ermentrout, G. B. n : m; phase-locking of weakly coupled oscillators. *Journal of Mathematical Biology 12* (1981), 327–342. 10.1007/BF00276920.

[9] Ermentrout, G. B., and Kopell, N. Oscillator death in systems of coupled neural oscillators. *SIAM J. Appl. Math. 50*, 1 (Jan. 1990), 125–146.

[10] Gibson, J. R., Beierlein, M., and Connors, B. W. Functional properties of electrical synapses between inhibitory interneurons of neocortical layer 4. *Journal of Neurophysiology 93*, 1 (2005), 467–480.

[11] Hodgkin, A. L. The local electric changes associated with repetitive action in a non-medullated axon. *The Journal of physiology 107*, 2 (Mar. 1948), 165–181.

[12] Juusola, M., Robinson, H. P. C., and de Polavieja, G. G. Coding with spike shapes and graded potentials in cortical networks. *Bioessays 29*, 2 (2007), 178–87.

[13] Koch, C., and Segev, I. The role of single neurons in information processing. *Nat Neurosci 3 Suppl* (2000), 1171–7+.

[14] Lánský, P., and Rodriguez, R. The spatial properties of a model neuron increase its coding range. *Biological Cybernetics 81* (1999), 161–167.

[15] Lewis, T. J., and Rinzel, J. Dynamics of spiking neurons connected by both inhibitory and electrical coupling. *J. Comp. Neurosci 14* (2003), 283–309.

[16] Lewis, T. J., and Rinzel, J. Dendritic effects in networks of electrically coupled fast-spiking interneurons. *Neurocomputing 58-60* (2004), 145–150.

[17] Mainen, Z. F., and Sejnowski, T. J. Influence of dendritic structure on firing pattern in model neocortical neurons. *Nature 382*, 6589 (July 1996), 363–6.

[18] Michael Beierlein, Jay R. Gibson, B. W. C. A network of electrically coupled interneurons drives synchronized inhibition in neocortex, 2000.

[19] Rall, W. Branching dendritic trees and motoneuron membrane resistivity. *Experimental Neurology 1*, 5 (1959), 491–527.

[20] Schultheiss, N., Prinz, A., and Butera, R. *Phase Response Curves in Neuroscience: Theory, Experiment, and Analysis*. Springer Series in Computational Neuroscience. Springer, 2012.

[21] Schwemmer, M., and Lewis, T. The robustness of phase-locking in neurons with dendro-dendritic electrical coupling. *Journal of Mathematical Biology* (2012), 1–38.

[22] Schwemmer, M. A., and Lewis, T. J. Effects of dendritic load on the firing frequency of oscillating neurons. *Phys Rev E Stat Nonlin Soft Matter Phys 83*, 3 Pt 1 (2011), 031906.

[23] Schwemmer, M. A., and Lewis, T. J. Bistability in a leaky integrate-and-fire neuron with a passive dendrite. *SIAM J. Applied Dynamical Systems 11*, 1 (2012), 507–539.

[24] Schwemmer, M. A., and Lewis, T. J. The theory of weakly coupled oscillators. *Phase Response Curves in Neuroscience, N.W. Schultheiss, A. Prinz, and R. Butera, eds., Springer 6* (2012), 3–31.